

POLITECNICO DI TORINO

Department of Mechanical and Aerospace Engineering

Master's Degree in Mechanical Engineering

Master of Science Thesis

**Automatic Test Equipment structure's mass
reduction through topology optimization
processes**



Advisor

Giorgio Chiandussi

Co-advisor

Andrea Tridello

Candidate

Giorgio Arcuri

December 2019

Table of contents

- Abstract 1
- 1. About SPEA.....3
 - 1.1. History of Spea [2] 3
 - 1.2. Technological environment5
- 2. Equipment’s chassis..... 6
 - 2.1. Evolution of the equipment’s chassis.....6
 - 2.2. Why Granite? 8
 - 2.3. Granite used for the structures 9
- 3. Structural Optimization..... 10
 - 3.1. Evolution of the design process 10
 - 3.2. The definition of “Optimum” 12
 - 3.3. Types of structural optimization 13
- 4. Case study 15
 - 4.1. Original Model..... 15
 - 4.2. Loads and support definition 18
 - 4.3. Frequency and Linear Static analysis..... 20
 - 4.3.1. Frequency analysis 20
 - 4.3.2. Linear static analysis..... 25
- 5. Topology optimization process..... 30
 - 5.1. Design and Non-Design space definition 30
 - 5.1.1. Non-design space 30
 - 5.1.2. Design space..... 31
 - 5.1.3. Model 1 – Full re-design 31
 - 5.1.4. Model 2 – Inspection window 34

5.1.5. Model 3 – Main cell	35
5.2. Set-up of the optimization’s parameters	38
6. Results.....	40
6.1. Iso-density curves results’ interpretation.....	40
6.2. Model 1.....	41
6.3. Model 2.....	43
6.4. Model 3.....	48
7. Re-construction and analysis of the optimized model	56
7.1. Aluminium structure	57
7.2. Aluminium structure V2.....	59
7.3. Aluminium structure V3.....	61
7.4. Hybrid structure.....	63
8. Conclusions	67
Bibliography	68

List of Figures

Figure 1 - The Flying Probe 4040.....	3
Figure 2 - FlyingProbe 4080.....	5
Figure 3 - 4060's Chassis.....	6
Figure 4 - 4020's Chassis.....	7
Figure 5 - 4050's Chassis.....	7
Figure 6 - 4080's Chassis.....	8
Figure 7 – Design cycle: a) conventional CAx tools, b) ODDP integrated with CAx [6].....	12
Figure 8 – a) Size optimization, b) Shape optimization, c) Topology optimization [7].....	14
Figure 9 - Orthogonal views: a) Side; b) Front; c) Top.....	15
Figure 10 - Isometric view.....	16
Figure 11 - Structure's sub-assemblies.....	17
Figure 12 – Plate dimensions.....	17
Figure 13 – Column and support base dimensions.....	17
Figure 14 - Bottom plate guideways.....	18
Figure 15 - Bottom plate with loads.....	19
Figure 16 - Frequency analysis model.....	21
Figure 17 - Frequency vs. Effective Mass Participation Factor.....	24
Figure 18 - Static analysis model.....	26
Figure 19 - Resultant displacement contour.....	27
Figure 20 - Deformed shape under the effect of the loads.....	27
Figure 21 - Von Mises stress contour plot.....	28
Figure 22 – Re-scaled VM stress contour.....	28
Figure 23 - Factor of safety.....	29
Figure 24 – Model 1 – Non-design space.....	32
Figure 25 – Model 1 – Design space – Isometric view.....	32

Figure 26 - Model 1 – Design space – Orthogonal views.....	33
Figure 27 - Model 2 – Inspection window	34
Figure 28 – Model 2 - Window's dimension	35
Figure 29 – Model 3 - Main cell	36
Figure 30 - Model 3 - Non-design space	36
Figure 31 - Model 3 - Orthogonal views	37
Figure 32 - Model 3 - Window's dimensions	37
Figure 33 – Stiffness maximization parameters.....	38
Figure 34 - Mass minimization parameters.....	39
Figure 35 - Shape explorer.....	40
Figure 36 - Optimized shape for different cut-off values: a) 0.8; b) 0.5; c) 0.3.....	41
Figure 37 - Model 1 - 0.5 cut-off value - Deformed shape	41
Figure 38 - Model 1 - 0.5 cut-off value - Orthogonal views.....	42
Figure 39- Model 2 - maxstiff20% – Orthogonal views.....	43
Figure 40 - Model 2 - maxstiff20% - Isometric view	44
Figure 41 - Model 2 - maxstiff10% - Orthogonal views.....	44
Figure 42 - Model 2 - maxstiff10% - Isometric view	45
Figure 43 - Shape controls description [6].....	46
Figure 44 - Symmetry shape control: a) Upper DS (cell); b) Lower DS (support base)....	46
Figure 45 - Model 2 - maxstiff10%_shapecontrol - Orthogonal views	47
Figure 46 - Model 2 - maxstiff10%_shapecontrol - Isometric view	47
Figure 47 - Model 3 - maxstiff20% - Orthogonal views.....	49
Figure 48 - Model 3 - maxstiff20% - Isometric view	49
Figure 49 - Model 3 - maxstiff10% - Orthogonal views.....	50
Figure 50 - Model 3 - maxstiff10% - Isometric view	50
Figure 51 - Model 3.1 - Design space - Window's dimension.....	51

Figure 52 - Model 3.1 - maxstiff20% - Orthogonal views	51
Figure 53 - Model 3.1 - maxstiff20% - Isometric view	51
Figure 54 - Model 3.1 - maxstiff10% - Orthogonal views	52
Figure 55 - Model 3.1 - maxstiff10% - Isometric view	52
Figure 56 - Support base optimization	53
Figure 57 - Support base optimization - Design space's dimensions.....	53
Figure 58 - Support base opt - maxstiff20% - Orthogonal views	54
Figure 59 - Support base opt - maxstiff20% - Isometric view	54
Figure 60 - Support base opt - maxstiff10% - Orthogonal views	55
Figure 61-Support base opt - maxstiff10% - Isometric view	55
Figure 62 - Al structure – Isometric view	57
Figure 63 - Al structure - Orthogonal views.....	57
Figure 64 - Pillar and support base block's dimensions	58
Figure 65 - Tilted elements - Geometry and dimensions.....	58
Figure 66 - Al structure V2 - Top and bottom plate's dimensions	59
Figure 67 - Al structure V2 - Orthogonal views.....	60
Figure 68 - Al structure V2 - Isometric view.....	60
Figure 69 - Al structure V3 - Components' dimension.....	61
Figure 70- Al structure V3 - Orthogonal views	62
Figure 71- Al structure V3 - Isometric view.....	62
Figure 72 - Hybrid structure - Component's dimensions	64
Figure 73- Hybrid structure - Orthogonal views.....	64
Figure 74 - Hybrid structure - Isometric view	65

List of tables

Table 1 - Properties of granite.....	10
Table 2 - Cumulative Effective Mass Participation Factor.....	22
Table 3 - Natural frequencies and EMPF.....	23
Table 4 - Mechanical performances of the original structure.....	29
Table 5 - Comparison between Granite and Aluminum 6061-T6	33
Table 6 - Models' comparison for different cut-off values	42
Table 7 - Mechanical properties of model 2's resultant geometries	48
Table 8 - Mechanical properties of the optimized structure's concept.....	56
Table 9 - Physical and Mechanical properties of 5083 Al-alloy	59
Table 10 - Natural frequencies comparison.....	65
Table 11 - Final solutions' performances comparison.....	66

Abstract

Nowadays, electronics surrounds every aspect of our life and almost every device has got an electronic board installed. From vehicles to smartphones, from tablets to the most complex aerospace, medical and military devices, this is a world guided by the continuous discovery of new technologies, which implies a continuous evolution of the systems utilized for the automatic testing of semiconductors, MEMS and electronic boards.

In engineering practice, the need to decrease the mass of a structure, preserving an adequate stiffness and resistance is often highlighted. One of the simplest and traditional solutions would be the choice of a different material, lighter, and at the same time, with higher mechanical properties with respect to the one previously used. Unfortunately, this solution is frequently related to an increase in the cost of the material, which make this option not always viable. The question now would be: is there another way to reduce the mass of a structure while maintaining its mechanical characteristics, in terms of strength and stiffness? The answer can be found in what are called optimization processes. The term “optimization” is related to the process of making something as good or effective as possible.[1]. Optimization processes take place by trying to minimize or maximize certain quantities without violating any of the constraints set by the problem itself. In the past, these were trial and error processes, but nowadays, thanks to the development of computational tools based on the optimization theory, it is possible to reach such goal in a more automatic way, achieving also high costs saving in the design process and avoiding the production of several prototypes.

The aim of this thesis is the study of the mass reduction of the structure, by means of topology optimization processes, of some automated test equipment (ATE) for assembled electronic boards (PCBAs) and modules, designed and manufactured by SPEA, one of the global leaders in this high-tech field.

Starting from the original model and knowing its mechanical characteristics it was possible to find some parameters to set as benchmarks in order to be able to compare the results obtained by means of the topology optimization process.

The results of such a process, which can be subdivided into five main stages, were then analyzed and a set of final manufacturable solutions, capable to meet the request of being lighter but at the same time comparable in terms of displacement was presented.

A comparison between the performances of the original model and the proposed solutions was finally made in order to be able to decide which can be chosen to be further improved and then produced.

1. About SPEA

1.1. History of Spea [2]

The 1970s witnessed an explosion in the understanding of solid-state physics, driven by the development of the integrated circuit and the born of modern computing with an increase in the use of personal computers. In 1976, Luciano Bonaria, a test engineer working at General Electric, created his own business, founding SPEA, systems for electronic and application. His idea was to design and manufacture standard equipment for testing electronic devices. The headquarters are located in Volpiano (TO), and in its year of birth, SPEA releases its first product, the INCIT.

At the end of the 70s, the first multi-functional tester for electronic boards was produced by SPEA, which started to expand its business abroad.

During the 80s several important products were produced: Digitest, the first Digital ICT Automatic Board Tester; Unitest 500, the first model with multi-function architecture, which laid the groundwork for all future production; and Comptest MX 500, designed for the emerging semiconductor technology of the Soviet Union, which was the first water-cooled equipment for testing microchips.

Moreover, during these years SPEA became well-recognized worldwide, started running its R&D department at full capacity, and its products were used for the first time in semiconductor testing. A few years later the worldwide USA/Japan monopoly (in the microchip testing market) was broken by SPEA, which entered officially in that market.



Figure 1 - The Flying Probe 4040

In 1996 *SPEA* became the fourth company in the world in the field of board testers, for which the *4040* was the flagship product, able to test high-density electric boards with flying probe system, a technology with better performances (five times better than competitors), very high speed and extreme mechanical precision.

The new millennium brought new changes in the markets of technology and electronics, and *SPEA* took the chance to increase its sales, gaining prestigious customers, including electronics manufacturers all around the world.

In 2003, were designed and produced two handlers: the H1000, the first handler for testing components mounted on reels; and the H3000, Pick & Place Handler for testing microchips on trays that found their application in the MEMS testing market.

In 2008 *SPEA* manufactured the H3560, high-productivity pick & place handler. During the same year, the C600MX (high pin count mixed-signal tester), and the STC Series (smart card module test cells) were presented. Successively, the Tri-Temp Option was released, thanks to that the MEMS test cells are able to apply the thermal conditioning to perform the test at three different temperatures, a strategic point for the automotive market.

In 2010, *SPEA* brilliantly overcame the global crisis, also thanks to its successful products: a new set of flying probe tester (4060-4020-4030) and PMTC Series test cells for power modules. During these years, 65% of the global ATE was represented by MEMS testing and in 2011 *SPEA* was the No. 1 company in the world in the testing of inertial MEMS such as gyroscopes and accelerometers

After becoming a leader in this market for quality, *SPEA* followed a cost-leadership strategy, by releasing the DOT (Oriented Device Tester), a new tester that has been able to reduce the unit cost of testing of MEMS; and the 3030 Benchtop, the fastest ICT tester in the world.

In 2015 the new pick & place test handler improved the throughput, which increases up to 33000 units per hour, also improvements in terms of MEMS stimulus are done, in such a way that a big variety of devices can be tested (inertial sensors, humidity sensors, pressure sensors, UV sensors, proximity sensors, MEMS microphones, magnetic sensors, combo sensors, and other IC devices).

In 2016 *SPEA* launched the 4080, an 8-axes dual side flying probe tester; this model is the first with a granite chassis, which offers low vibration and thermal stability, reflecting over the probing precision, which was better than ever.



Figure 2 - FlyingProbe 4080

Nowadays SPEA is the undisputed leader in Europe and second in the world in testing electronic boards, and No. 1 in the world of inertial MEMS testing. With more than 8600 systems installed in 85 countries, in 2017 the firm billed more than € 111 million of revenues, of which the 20% is invested in R&D.

1.2. Technological environment

The field of ATE is very wide, and, due to the huge diffusion of electronic devices, it is a strong and solid market. The list of possible applications of ATE is already big, but in particular, *SPEA* focuses its development in testing systems for electronic boards and MEMS, which stands for micro-electro-mechanical systems. The first one is a printed circuit board that supports electronic components like resistors, capacitors, and inductors, and connects them using conductive tracks. The latter consists of a set of devices of different nature (mechanic, electric, electronic), integrated on a substrate of semiconductor material, usually silicon.

MEMS have been considered one of the most promising technologies of the XXI century. The order of magnitude for the dimensions of these devices is of micrometres and finds application in very different fields (industrial, automotive, military, white goods, medical, etc.).

Typically, an ATE system uses an automated placement tool, the “handler”, which mechanically places the device to be tested in a test interface, so that the device can be measured by the equipment. Measurements made on the device are usually calculated, stored and analyzed by some form of computer. ATE systems can test a wide range of electronic devices and systems and its scope is to reduce the amount of test time needed to verify the work of a particular device, so that faults can be recognized before the product goes at the end of a final consumer, and to exclude a possible human error from the testing phase.

2. Equipment’s chassis

2.1. Evolution of the equipment’s chassis

For the purpose of the analysis of the evolution of the chassis’ type, the focus is maintained on one of the types of systems designed in the firm, the Flying Probe Tester. This type of machines consists of a series of probes that move rapidly along the X, Y and Z direction and performs their tasks with high mechanical speed, extreme accuracy and single or dual-side probing capability.

The first one to analyze is the chassis of the 4060 model. It is made of cast iron profiles and, as it can be seen from figure 3, it consists of four pillars, fixed to a reinforced bed and jointed together to horizontal members by means of electro slag welding. In order to increase the stiffness, support components were placed to maintain the vertical pillar fixed with respect to the horizontal component. This kind of structure has been designed in order to cope with the vibration caused by the high acceleration rate of the axes, in particular, the Z-axis that reaches an acceleration rate of 10g.

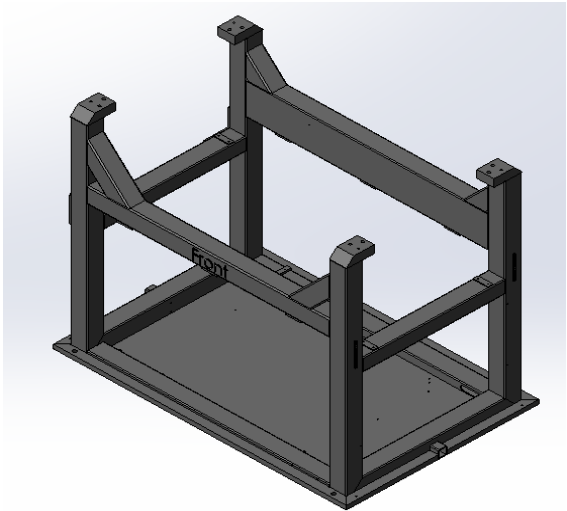


Figure 3 - 4060's Chassis

The successive types of chassis belong to the 4020 and 4030 models which are made by cast-iron sheets, folded and spot-welded. This solution resulted to have lower stiffness and presented problems of bending during operating conditions. In order to solve this problem, the 4030 model was born, in which the tubular structure of the pillar was filled with a polymeric compound, in order to increase the weight and in this way reduce the problem of deflection of the structure. Unfortunately, the problem was not completely solved, due to the lack of stiffness in the bottom part of the structure.

The 4050's chassis presents a hybrid structure, made by tubular cast iron components and presents more or less the same structure of the 4060 with four pillars, fixed to the base and jointed together at the top and at the centre by means of horizontal members, in order to provide a higher stiffness. This chassis was meant to be lighter than the 4060's one since the application required from this model does not require a higher dynamic load, given from the lower acceleration rate of the axes,

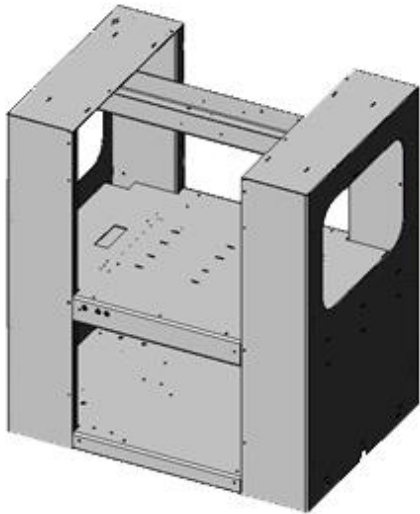


Figure 4 - 4020's Chassis

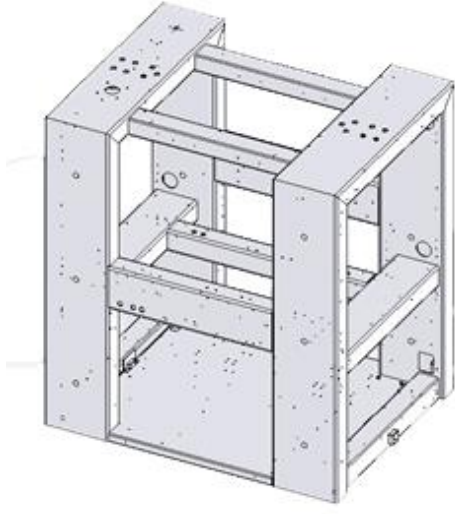


Figure 5 - 4050's Chassis

The last type belongs to the 4080 model. It presents an innovative granite chassis that offers low vibration and thermal stability, ensuring very high probing precision at ultra-fast test speed. It consists of a top and a bottom slab, connected by four pillars. There are also present some supports at the interface between the pillars and the top and bottom slabs in order to increase the rigidity of the structure.

The technology installed on this machine makes the axes move at an acceleration rate reaching 30g, so this kind of solution allows having the best performances considering the real operating conditions.

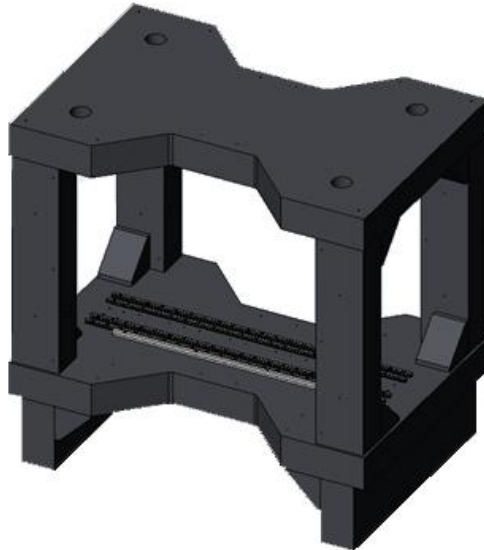


Figure 6 - 4080's Chassis

2.2. Why Granite?

Granite is a common, coarse-grained, hard igneous rock consisting chiefly of quartz, orthoclase or microcline, and mica.[3]

Due to the requirement of an always increasing precision and repeatability of the tests done, and due to the increasing speed of the testing process, the need for an elevated dimensional accuracy of the frame has been identified. Furthermore, due to the requirement of an increased level of stiffness and damping capacity in order to cope with the vibration caused by the elevated acceleration/deceleration rate of the axes and the need to maintain the operational accuracy, the choice made was to use the granite as material to build the chassis.

The granite, thanks to its properties, has recently found a very large use both in the field of traditional measurement tools and for the newest coordinate measuring machines, due to the very high surface finishing precision obtainable by means of the lapping process that allows achieving surfaces' flatness higher than any other material.

There are other reasons that induce to choose the granite for the construction of systems that require very high precision, as like as:

- Dimensional stability, since there is no presence of internal stresses
- Thermal stability, due to its very low linear expansion coefficient
- Hardness
- Wear resistance
- Acid and erosion resistance
- Non-magnetic properties
- Oxidation resistance
- Electrical insulation

Compared to conventional iron or steel, natural granite offers best damping characteristics and thermal stability, so to minimize the effect of vibrations and deformations that would affect accuracy and reliability through time.

2.3. Granite used for the structures

Nowadays SPEA produces three models with the chassis made of granite, and are actually used two different kinds of material: Africa Black granite and Ghiandone Sardo also called Bianco Sardo. Those two are natural granites, directly extracted from the quarries and the processed in order to obtain the final product.

The supplier is a leader in Europe for the production of precision granite instruments and high precision granite structures and bases for different sectors such as machine tools, CMM (coordinate measuring machines), optical machines, micro-electronic machines, test benches, circuit boards drilling machines and precision components for automotive, aerospace and industrial markets.

In the following tables are listed the most relevant features of the granite used, given by the supplier:

Granite's chemical and physical properties			
	Africa Black	Bianco Sardo	Synthetic
Density [kg/dm³]	2.85	2.63	2.3
Young Modulus [GPa]	60-105	50	30-40
Tensile strength [MPa]	24	20	10-15
Compressive strength [MPa]	244	184	120-150
Linear expansion coefficient [m/m °C]	6.5*10 ⁻⁶	6.5*10 ⁻⁶	10-15*10 ⁻⁶
Thermal conductivity [W/m K]	2	2	1-3

Table 1 - Properties of granite

As we can see from Table 1, the Africa Black granite presents higher mechanical properties with respect to the Bianco Sardo one, and for this reason, it is used for the application that requires better performances.

Another solution given by the supplier was to use a synthetic granite, which is a composite material made up of a mixture of specific granite aggregates of different grain sizes, bonded with epoxy resin and hardener. This granite is formed by casting into moulds, reducing the costs because of the much simpler manufacturing process.

Even if it is a cheaper solution, as we can see from the comparison with the natural granite, it presents much lower mechanical properties, which make it not adequate for the required applications.

3. Structural Optimization

3.1. Evolution of the design process

As J.G.Gordon suggested, a structure is defined as “any assemblage of materials which is intended to sustain load” [4]. Therefore, structural optimization can be seen as the subject that studies a way by which an assemblage of materials sustains load in the best way. In the past, the validation of the design during the product development stage was obtained by means of tests on prototypes and from the results obtained, the designer would have

made the due changes to the initial design in an absolute empirical way. Therefore, in order to obtain the desired final design, a lot of changes and tests on different prototypes would have been necessary, thus requiring many resources in terms of personnel, time and money. Nowadays the product's life cycle is getting shorter and shorter and there is an always-tightening request for lighter products, so in order to cope with this kind of constraints, the designer can make use of a particular tool such as the Computer-Aided Design and Simulation (CAx). Computer-aided technologies are the use of computer technology to aid in the design, analysis, and manufacture of products. Advanced CAx tools merge many different aspects of the product lifecycle management (PLM), including design, finite element analysis (FEA), manufacturing and production planning.[5].

The most relevant instruments of the CAx are: CAD (Computer-Aided Design) and CAE (Computer-Aided Engineering); the first is the use of computer as aid in the processes of creation and design of a 2D or 3D geometry, and the latter is the use of computer software as aid to the solving of engineering problem by means of numerical modelling. Thanks to the CAx, it is possible to simulate the behaviour of the product subjected to the real operational conditions in a virtual environment and then use the results obtained in order to redefine the design in an iterative way. This type of approach helps to reduce the costs and the time during the product development but the designer would have to rely on experience or insight to come up with proposals. The analysis tool is then used to evaluate each proposal, with the designer using these analysis results or responses to choose the "best".

Relatively recent advances in mechanics and software have provided numerical codes, based on different optimization techniques, which allows to automatically modifying the original geometry and, at the same time, perform the analysis. In other words, the software can suggest the design that is best suited to the conditions you specify, managing to obtain as a result, an "optimum" design. This is the so-called Optimization Driven Design Process (ODDP).[6]

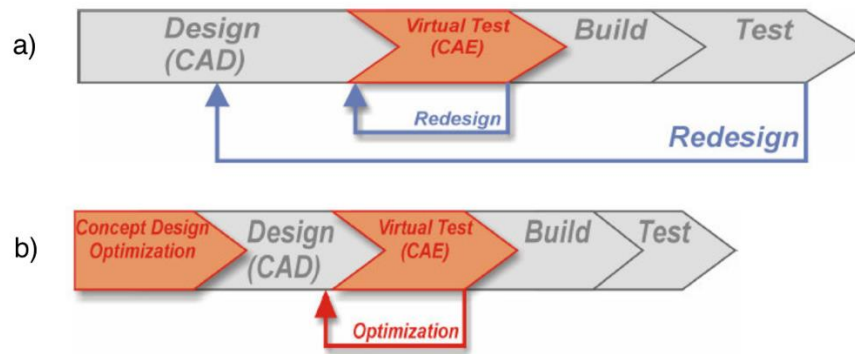


Figure 7 – Design cycle: a) conventional CAx tools, b) ODDP integrated with CAx.[6]

As shown in Figure 7, thanks to the integration of Optimization Driven Design Process with CAx tools it is also possible to avoid the redesign stage of the product cycle, since the software automatically manages to find the best design, capable of overcoming the tests.

3.2. The definition of “Optimum”

The final goal of the designer is to obtain the optimum design taking into account all the given constraints. The definition of “Optimum”, proposed by the dictionary, is “the greatest degree or best result obtained or obtainable under specific conditions. What is important to define are these “specific conditions” which, in the engineering terms, correspond to the conditions that give the design freedom, or in other words, the capability to choose between different alternatives.

In order to define a problem in design optimization, it must be specified the design space, the design variables, the constraints, and the objective(s).

Since most components to design have to assemble with other components, they need to fit together. This means it is needed to define a package space within which they need to fit, and assembly points that cannot be varied since they are decided by other components. In mathematics, the package space is referred to as the design space or the optimization domain_[6].

The design variables are the structural parameters that are able to change during the optimization process. Typical examples include material properties, topology, and geometry of a structure and member sizes. Design variables can be continuous or discrete, depending on the type of optimization that is being performed.

The design constraints can be defined as restrictions imposed on a problem by cutting-off some of the values that selected response functions (a measurement of system performance) of the system can obtain and that must be satisfied for the design to be acceptable.

Finally, the objective or objectives are the quantitative parameters used to evaluate a design_[6]. In most of the real application, there are multiple and different objectives, which can also be contradictory, thus reducing the design freedom and forcing the designer to make a compromise.

In general, an optimization problem can be seen as the minimization of an objective function subject to a set of constraints. The corresponding mathematical statement is:

$$\begin{aligned} & \min_x f(x) \\ & \text{Subject to } g_j(x) \leq 0 \quad \text{with } j=1, \dots, m \quad [6] \\ & \quad \quad \quad x_i^L \leq x_i \leq x_i^U \end{aligned}$$

where:

- $f(x)$ is the objective function;
- x is the vector of design variable;
- $g(x)$ are the constraint functions.

3.3. Types of structural optimization

In the structural engineering field, depending on which design variable is chosen, it is possible to distinguish three different types of optimization:

- a) Size optimization;
- b) Shape optimization;
- c) Topology optimization.

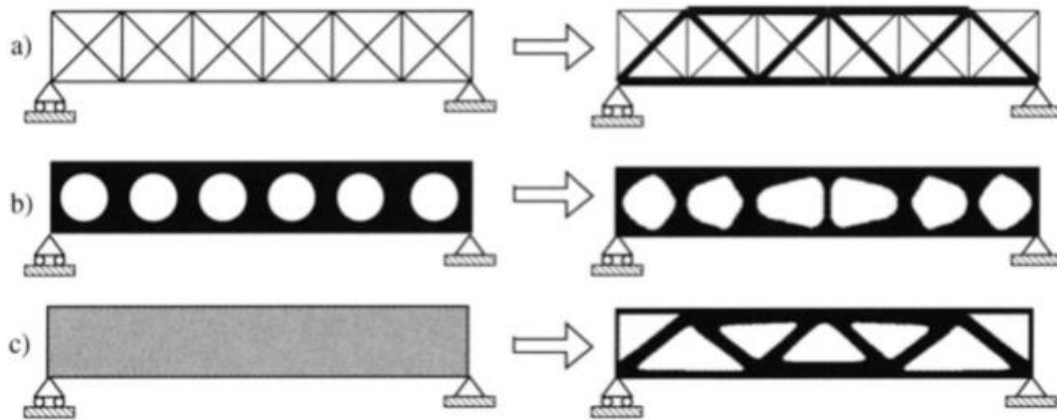


Figure 8 – a) Size optimization, b) Shape optimization, c) Topology optimization.[7]

Size optimization is the easiest type of structural optimization and consists mainly of changing the dimensions of the component. For example, the result can be the “best” cross-sectional area of a beam subjected to certain loads and support condition, so that a specific objective function (like the maximum stress, the stiffness or the deflection) results to be minimized (or maximized). The most important characteristic of size optimization is that the design domain is well known and does not change during the optimization process.

In a shape optimization problem, on the other hand, the design variable is the domain itself and the goal is to find the optimal shape of the domain, by changing, for example, the thickness of an element, the diameter of a hole or any other size of a characteristic element of the structure.

Finally, the most general of the three structural optimization types is topology optimization. It involves the determination of features such as the number, location and shape of holes and the connectivity of the domain. The purpose of topology optimization is to find the optimal layout of a structure within a specified region.[7]. In other words, it allows having the best distribution of material inside the domain.

4. Case study

4.1. Original Model

As already mentioned before, this thesis project is focused on the re-design of the structure of an ATE (Automatic Test Equipment) made completely by granite slabs of different shapes and dimensions connected to each other, of which in Figure 9 and 10 are reported the orthogonal and isometric views. The main goal is to reduce the mass of the whole structure trying to maintain unaltered or at least comparable its mechanical performances, and in order to fulfil it, a topology optimization problem was set up.

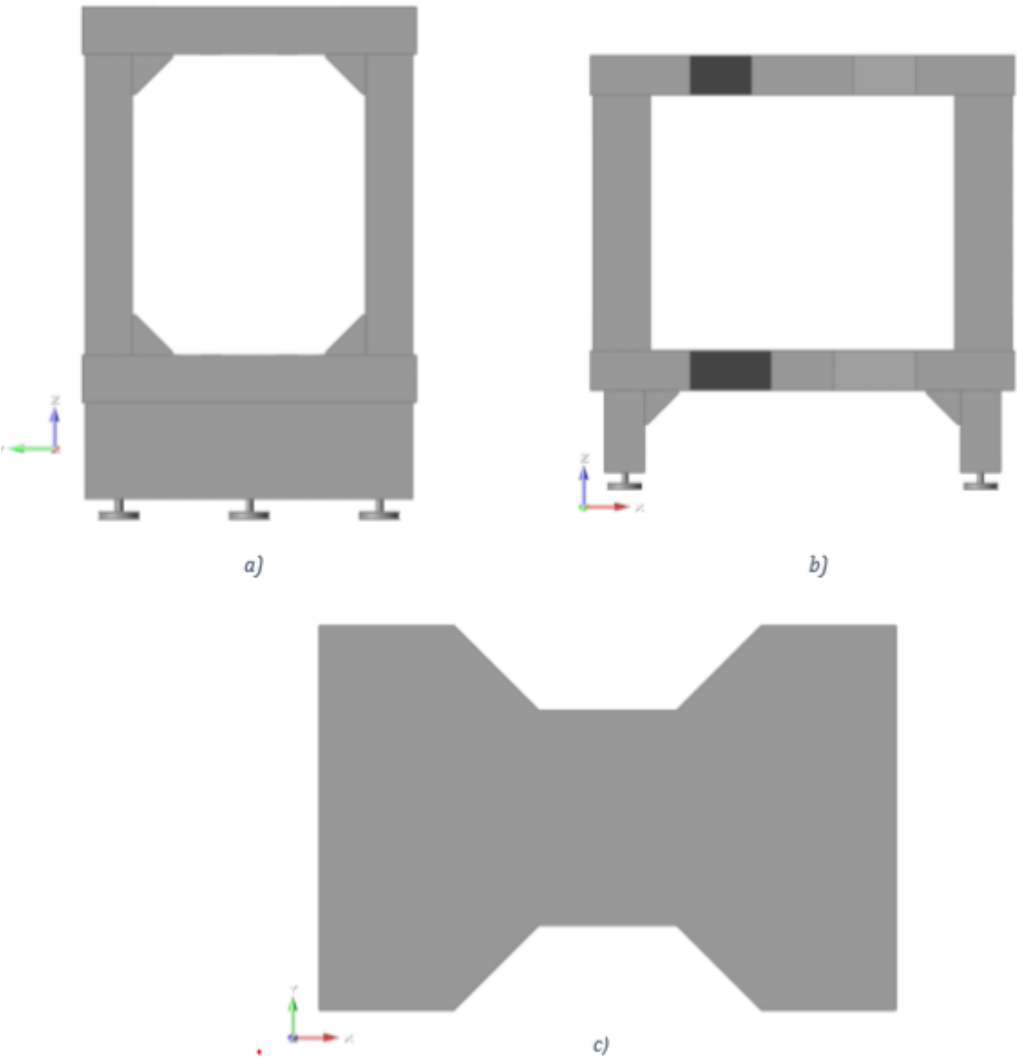


Figure 9 - Orthogonal views: a) Side; b) Front; c) Top

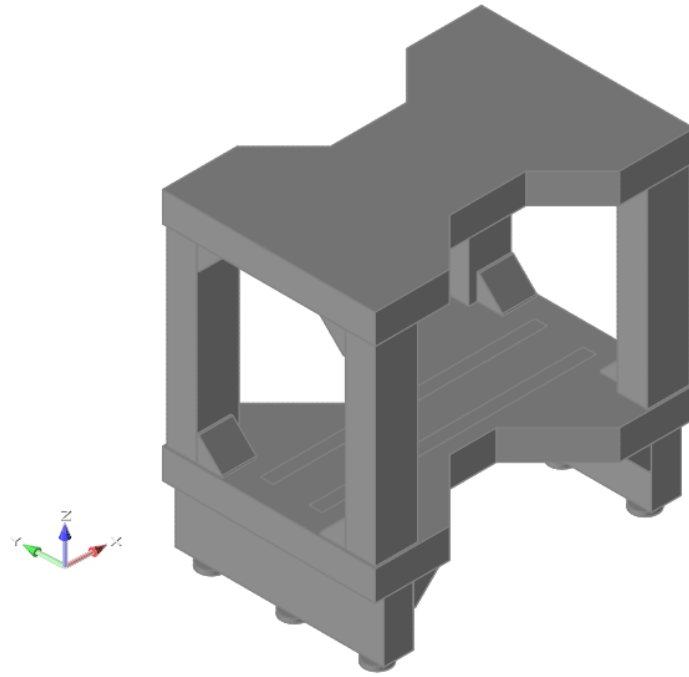


Figure 10 - Isometric view

As can be seen in Figure 11, the granite structure is made by two main sub-assemblies: the cell (coloured in light blue) and the support-base (coloured in brown). The whole structure is connected to the ground by means of six steel feet. The cell is composed of two horizontal slabs (1000 x 1500 x 140) mm, from now on identified with “bottom” and “top” plates, connected by four columns (906 x 200 x 140) mm and eight polyhedric support in order to provide higher rigidity between vertical and horizontal elements. The support base is made by two transversal slabs (980 x 290 x 140) mm and four polyhedric support. The connection between components is made by using modified epoxy-polyester resin-based glues. The most relevant dimensions are represented in Figure 12 and Figure 13.

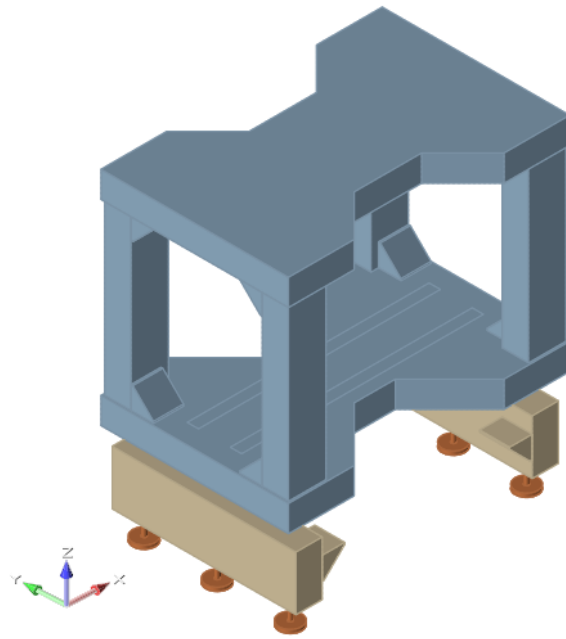


Figure 11 - Structure's sub-assemblies

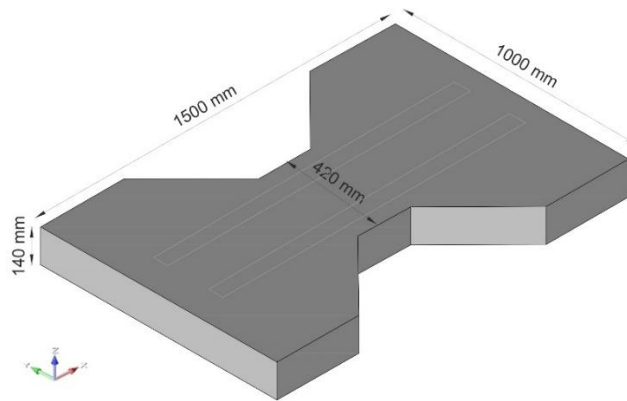


Figure 12 - Plate dimensions

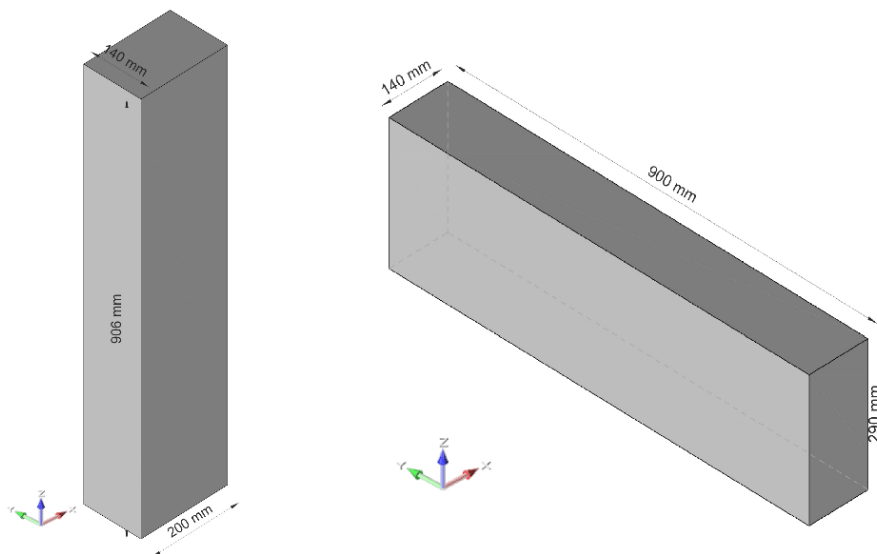


Figure 13 - Column and support base dimensions

Over one of the side of the top and bottom plate is mounted a couple of guideways which sustain, thanks to some slides, four axes that move in X, Y and Z direction at a different speed and acceleration rate, reaching very high values in the vertical direction,

4.2. Loads and support definition

In order to carry out the topology optimization, it is necessary to know the performances of the original structure, considering all the loads applied to it corresponding to the mass of the mechanical equipment moving onto a couple of profiled guideways mounted on the top side of the bottom plate and on the bottom side of the top plate of the structure. In Figure 14 is represented the bottom plate with the portion of the surface assigned to the guideways, over which the loads are distributed.

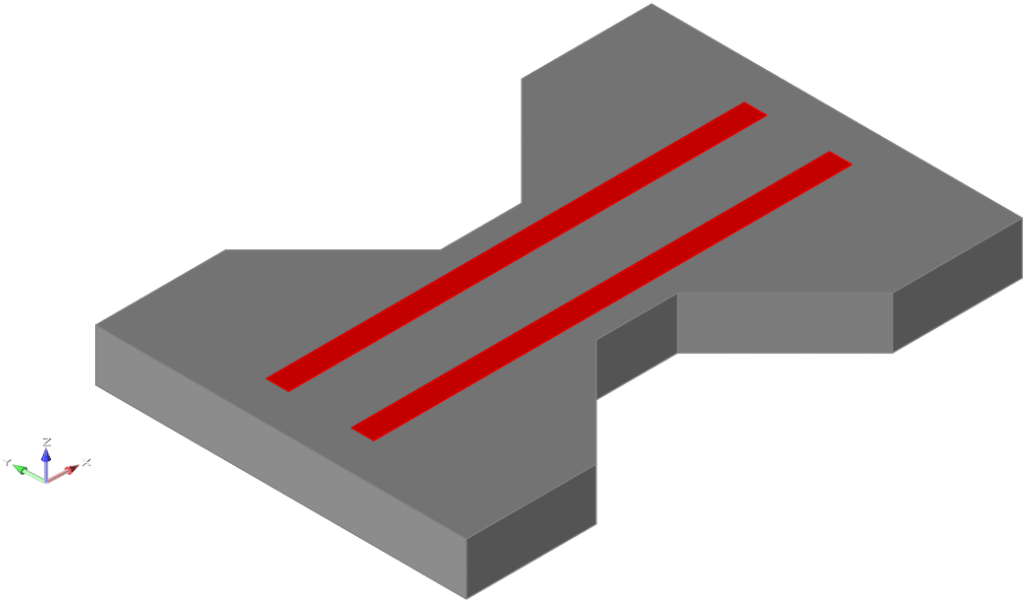


Figure 14 - Bottom plate guideways

The loads applied were calculated considering the forces with respect to the direction of motion of the axes and in particular, it was possible to distinguish for each of the two plates, four principal acting forces, each of them related to the mass of the tools and the equipment moving, multiplied by the relative acceleration rate and applied from the centre of gravity of the axes in their external-packed configuration to the surface of the guideways.

The values of the loads acting, shown in Figure 15, were computed in the following way:

- Load due to the motion in the X direction of the Y-axes at 3g acceleration rate acting

$$F_{xx} = 4 \cdot m_{xx} \cdot 3g \sim 870 \text{ N}$$

applied at 270 mm along X-direction, 130 mm along Z-direction from the centre of the plate.

- Load due to the motion in the X and Y-direction of Z-axes, Y-slides and relative brackets and tools at 3g acceleration rate

$$F_{xy} = 4 \cdot m_{xy} \cdot 3g \sim 380 \text{ N}$$

applied at 270 mm along X-direction, 130 mm along Z-direction and 220 mm along Y-direction from the centre of the plate.

- Load due to the motion in the Z-direction of Z-slides with the respective tools at 30g acceleration rate

$$F_{zz} = 4 \cdot m_{zz} \cdot 30g \sim 140 \text{ N}$$

applied at 270 mm along X-direction, 130 mm along Z-direction and 220 mm along Y-direction from the centre of the plate.

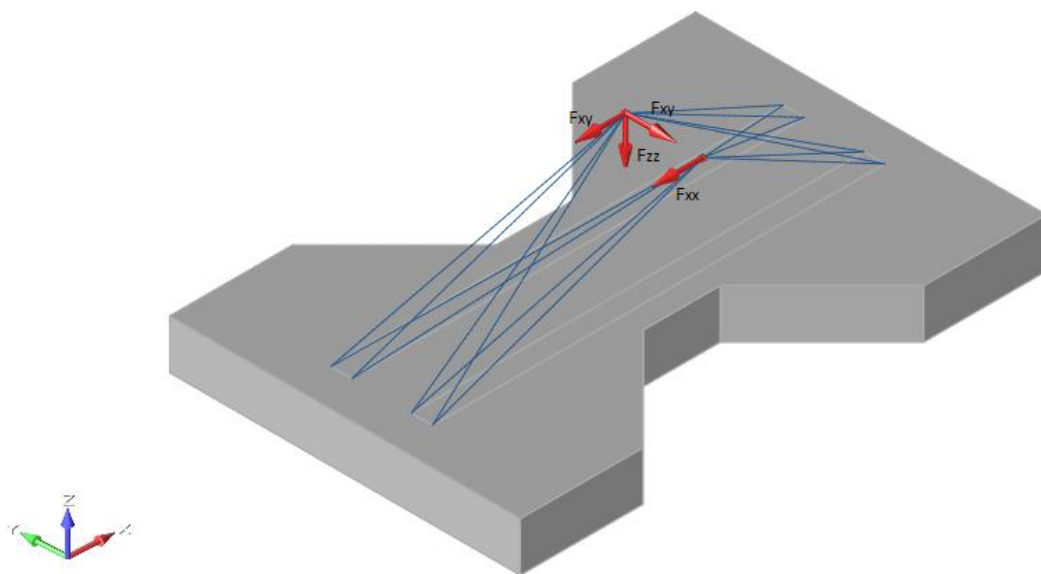


Figure 15 - Bottom plate with loads

4.3. Frequency and Linear Static analysis

The starting point for the process of optimization of the structure, once the loads acting on it are known, is to be aware of which is the response to them, in terms of displacement, mode shape and natural frequencies.

4.3.1. Frequency analysis

Every structure has a tendency to vibrate at a certain frequency if subjected to a disturbance, those frequencies are called natural frequencies and are in number equal to the degree of freedom of the structure. Each of the natural frequency is linked to a certain shape, called mode shape, which the structure tends to assume when oscillating at that frequency. Natural frequencies and mode shape are functions of the system geometry, material properties and support condition. The modal analysis allows knowing the natural frequencies of the system and consequently, by confronting the values obtained with the ones given from the dynamic loads acting on the system, to avoid the resonance phenomenon, which will cause undesired displacements and stresses leading to the damage of the structure.

The model used for the analysis is represented in Figure 16, in this case, in order to compute the natural frequencies, no loads were applied and, for each of the holes where the support feet are placed, a rigid fixed-geometry constraint was set, limiting the vertical and rotational motion.

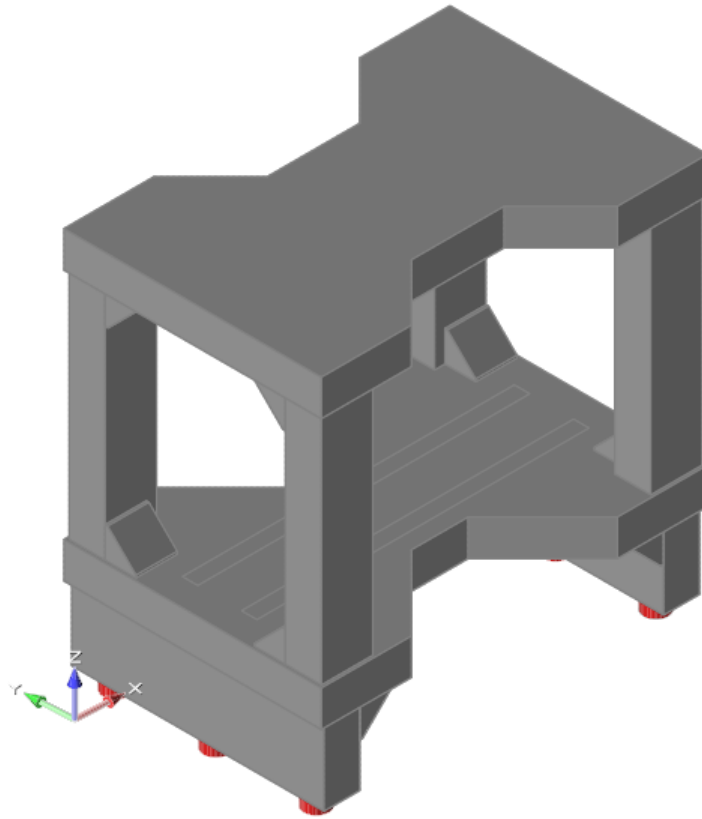


Figure 16 - Frequency analysis model

The results of the analysis were useful to understand at which frequencies and in which ways the structure would move when subjected to an external load. In this particular case, in Table 2 are listed the number of natural frequencies that allows having a cumulative equivalent mass participation factor (CEMPF) of at least 80% for each direction of motion, since, for the most of the cases, this is considered a reasonable threshold value.

Table 3, in the following page, reports the value of the first 30 modes with their respective natural frequencies and effective mass participation factor normalized with respect to the total mass, for each of the global axis. The effective mass participation factor represents the percentage of the system mass that participates in a particular mode and provides a measure of the energy contained within each resonant mode. Usually, a mode with a large EMPF value is a significant contributor to the dynamic response of a system.

Figure 17, instead, plot the effective mass participation factors (EMPF) for the global X, Y, and Z directions for each mode with respect to the mode number, to which is connected a specific natural frequency.

Mode number	Frequency [Hz]	X	Y	Z
1	51,4	57,0	0,0	0,0
2	62,3	57,0	47,5	0,0
3	88,3	57,0	47,5	0,0
4	183,9	57,0	47,5	24,9
5	251,1	82,6	47,5	24,9
6	298,8	82,6	51,2	24,9
7	303,0	82,6	51,2	54,7
8	316,7	83,4	51,2	54,7
9	370,7	83,4	51,2	54,7
10	393,3	83,4	59,1	54,7
11	429,0	83,4	65,1	54,7
12	430,3	83,4	65,1	54,7
13	477,7	83,4	65,1	54,7
14	493,4	84,1	65,1	54,7
15	500,4	84,1	65,1	54,8
16	507,0	84,1	78,4	54,8
17	554,1	84,1	78,4	54,8
18	567,5	84,1	78,4	79,3
19	570,3	88,6	78,4	79,3
20	575,5	88,6	78,4	79,3
21	721,4	89,9	78,4	79,3
22	733,1	89,9	78,5	79,3
23	745,8	89,9	78,5	79,8
24	757,5	91,8	78,5	79,8
25	762,6	91,8	81,1	79,8
26	785,0	91,8	81,1	79,8
27	814,3	91,8	81,1	80,8
28	828,2	92,5	81,1	80,8
29	839,3	92,5	81,1	80,8
30	849,8	92,5	90,9	80,8

Table 2 - Cumulative Effective Mass Participation Factor

It is remarkable to say that, for the X-direction, just the first five natural frequencies were enough to reach the mass participation threshold; instead, for the Y and Z direction, it was necessary to compute respectively until the 25th and 27th natural mode to reach the 80% of CEMPF.

Mode number	Frequency [Hz]	X [%]	Y [%]	Z [%]
1	51,39	57,0	0,0	0,0
2	62,25	0,0	47,5	0,0
3	88,27	0,0	0,0	0,0
4	183,90	0,0	0,0	24,9
5	251,12	25,6	0,0	0,0
6	298,80	0,0	3,6	0,0
7	302,97	0,0	0,0	29,8
8	316,66	0,7	0,0	0,0
9	370,69	0,0	0,0	0,0
10	393,27	0,0	8,0	0,0
11	429,00	0,0	5,9	0,0
12	430,32	0,0	0,0	0,0
13	477,67	0,0	0,0	0,0
14	493,40	0,7	0,0	0,0
15	500,41	0,0	0,0	0,1
16	506,99	0,0	13,4	0,0
17	554,13	0,0	0,0	0,0
18	567,45	0,0	0,0	24,6
19	570,29	4,5	0,0	0,0
20	575,51	0,0	0,0	0,0
21	721,39	1,3	0,0	0,0
22	733,12	0,0	0,0	0,0
23	745,84	0,0	0,0	0,5
24	757,47	2,0	0,0	0,0
25	762,63	0,0	2,7	0,0
26	784,99	0,0	0,0	0,0
27	814,26	0,0	0,0	1,0
28	828,24	0,6	0,0	0,0
29	839,34	0,0	0,0	0,0
30	849,76	0,0	9,7	0,0

Table 3 - Natural frequencies and EMPF

Table 3 allows also determining whether a mode is to be considered during the analysis, in fact, it may happen that the exciting frequency is close to one of the natural frequencies but the energy contained within this resonant mode is a small value and hence there is no need to worry about resonance effect. Therefore, in order to select the most effective modes, it is a common rule to consider only the ones with EMPF higher than 1% or 2%.

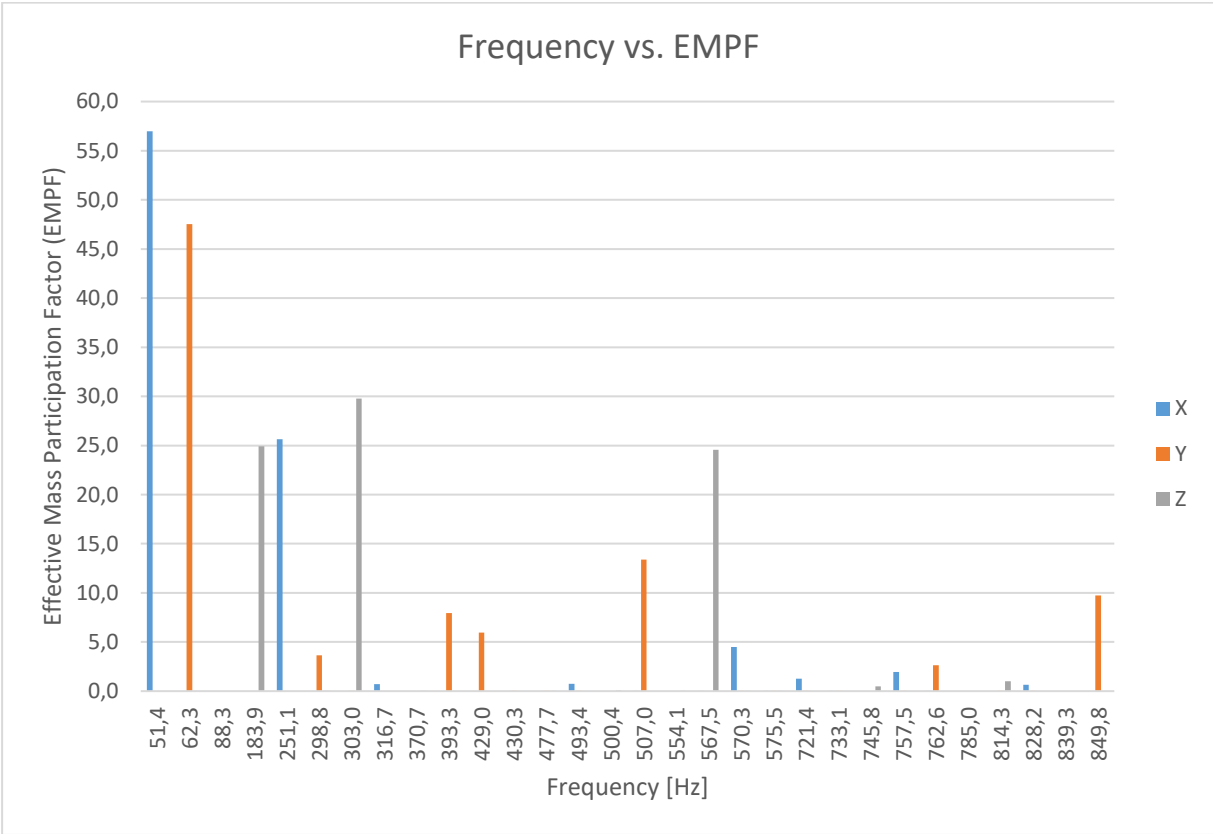


Figure 17 - Frequency vs. Effective Mass Participation Factor

Considering the data obtained from the modal analysis, and the ones given from SPEA about the response of the structure to the external load, it is possible to make some observations:

- Since the external load frequency range goes from 5 to 350 Hz it is possible to neglect the effect of the modes with a natural frequency out of this range, so the first eight modes are the one to be considered for further studies;
- Of these eight first modes, there are some that can be excluded due to the fact that their EMPF is lower than the 2% in each of the direction of motion, just like mode number 3 and 8, having respectively a natural frequency of 88.3 Hz and 316.7 Hz.

The data given from SPEA were collected during a characterization test made in the past, during the first stages of the born of the system. Those tests were performed by placing two accelerometer in two different point of the structure (usually top and bottom plate), evaluating the response of the structure to the external loads for the three different direction of motion. From the data obtained, it was possible to define a range of vibration registered, that goes from 5 Hz to 305 Hz, and that for each of the axes there were different peak values, for example:

- X-direction [Hz] : 19, 28, 37, 47 and 57;
- Y-direction [Hz] : 19, ,28, 39, 47, 58, 66, 76;
- Z-direction [Hz] : 18, 27, 39, 48, 56, 67, 74, 85, 95.

Those are approximate values extrapolated from some of the graphs handed out by the company.

Unfortunately, it has not been possible to determine in a precise way the value of the frequency of the external excitation, due to the fact that was not possible to install a set of accelerometers on the structure and make some experimental tests.

For this reason, the loads described in chapter 4.2 were considered as static loads and were used in order to perform a linear static analysis that is described meticulously in the next chapter.

4.3.2. Linear static analysis

Linear Static analysis calculates displacements, strains, stresses, and reaction forces under the effect of applied loads and has to be performed under two precise assumptions. First of all, there has to be a linear relationship between the force applied and the response of the system to such loads; and secondly, these loads have to be considered time-invariant or applied slowly and gradually until they reach their full magnitude without changing in direction during the analysis, which means that any inertial or damping forces due to impact or dynamic loading have to be neglected. There is also a third assumption, which states that all the induced displacement must be no more than the 0.2% of the initial length.

In Figure 18 is represented the model used for the static analysis, which differs from the one used for the frequency analysis only for the loads applied over the surface delimited by the linear guideways for both the top and the bottom plate, and for the addition of the six feet which support the granite structure, considered as non-deformable solid, having very high Young modulus and Yield stress values and very low density value. In this case, the support is applied on the circular bottom surface of each one of the six feet. It is important to mention that, for the purpose of this analysis, another load is added to the one reported in chapter 4.2, and it refers to the fact that the structure is also subjected to an acceleration of 1.5g in order to take into account of the mass of the instrument fastened to the structure.

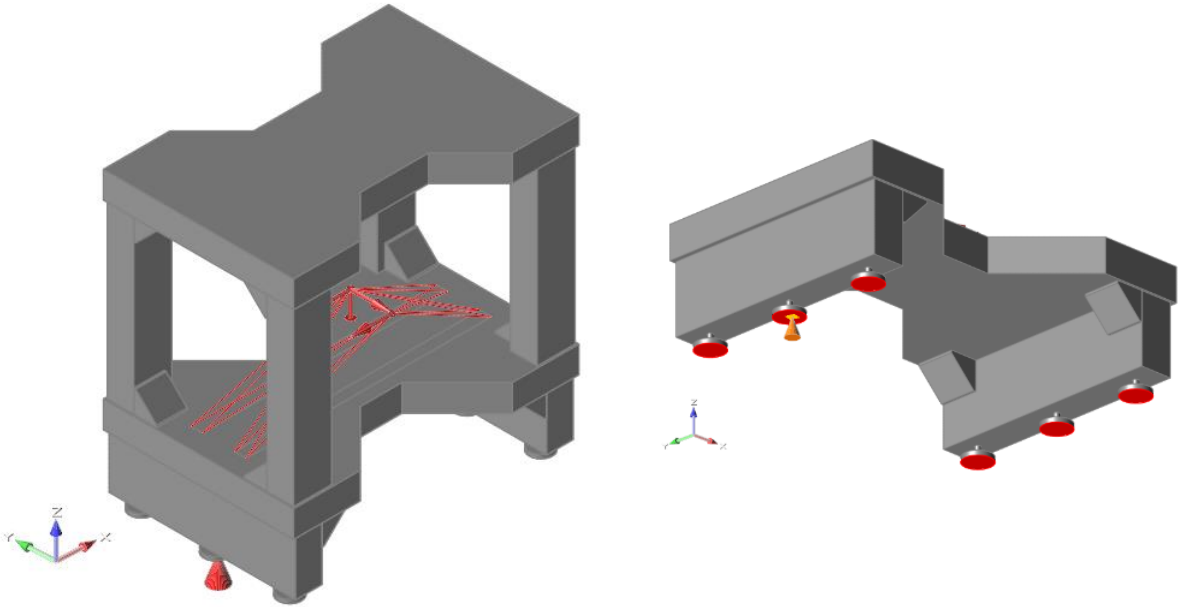


Figure 18 - Static analysis model

The main results to extrapolate from this analysis regards the values of displacement in each direction of motion and the resultant displacement, the latter is the one that from now on is to be taken as a comparison factor with the forthcoming solutions given as a result of the topology optimization. At the end of this chapter it is possible to examine the mechanical performances of the original structure, starting from the contour plot of the resultant displacement (see Figure 19) with the indication of the minimum and the maximum value, and continuing with the deformed shape under the effect of the loads (Figure 20), the contour plot of the Von Mises stress (Figure 21) and finally the factor of safety (Figure 23).

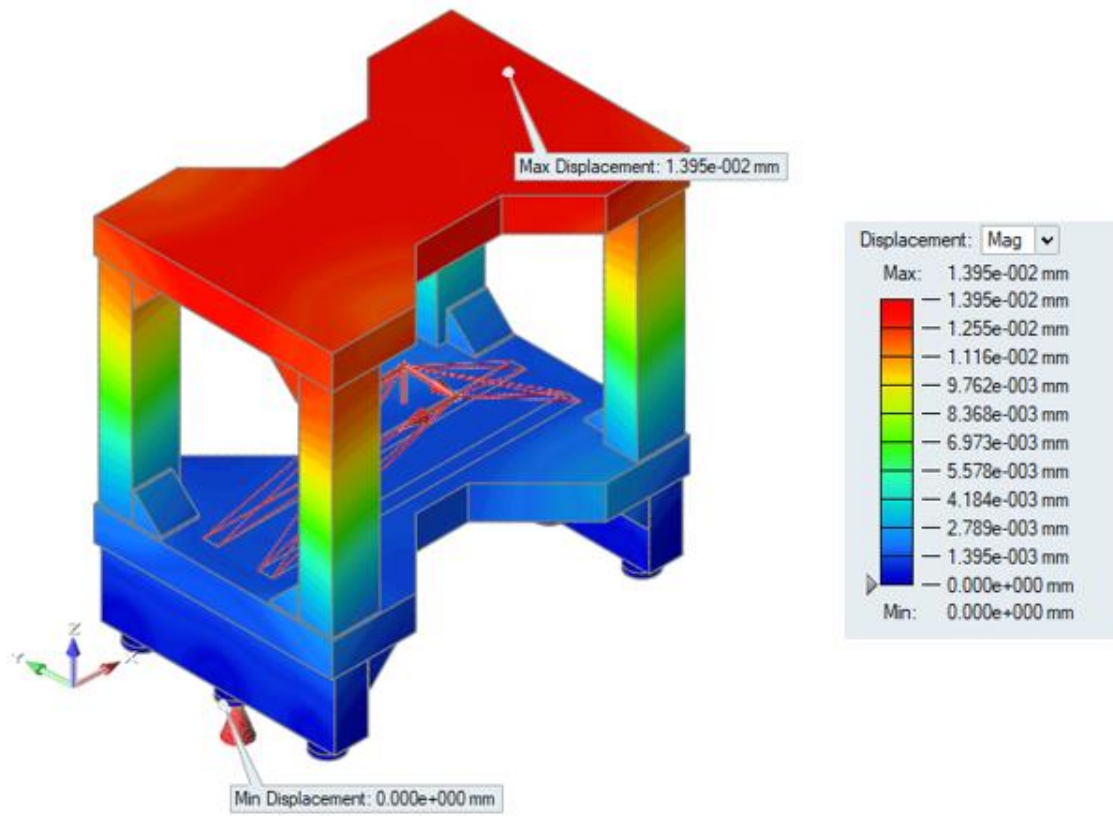


Figure 19 - Resultant displacement contour

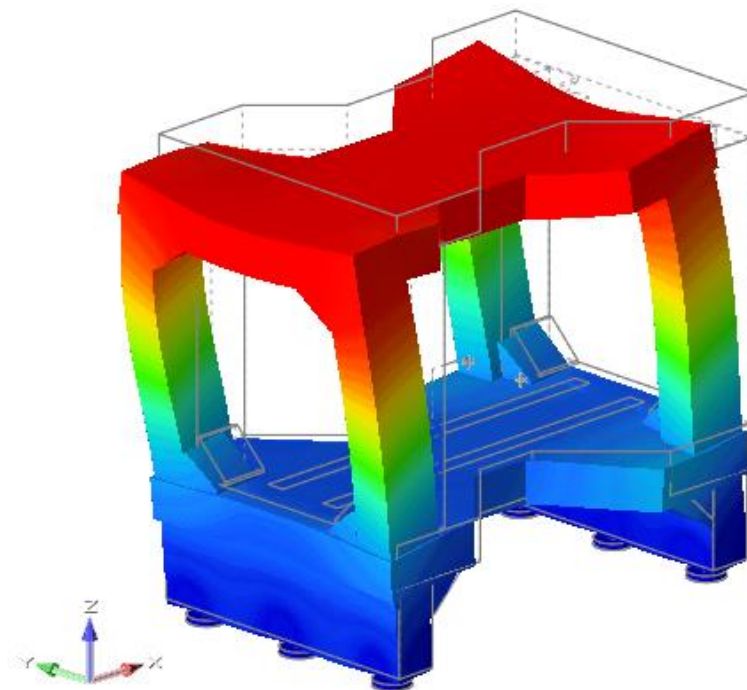


Figure 20 - Deformed shape under the effect of the loads

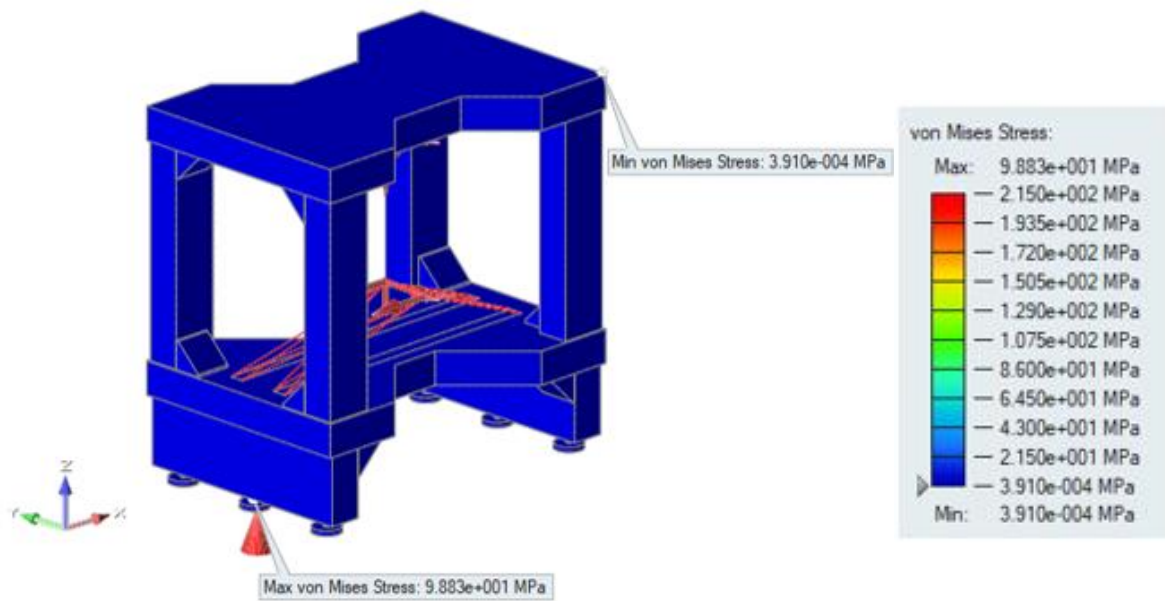


Figure 21 - Von Mises stress contour plot

From Figure 21 it is possible to see the big difference between the minimum and maximum value of the Von Mises stress, in fact, the max value is registered on the external surface of one of the six feet, which, as mentioned before, is simulated as a non-deformable body. So in order to understand which is the actual maximum stress on the granite structure, it is convenient to rescale the result considering as maximum threshold a value coherent with granite typical behaviour, in this case, equal to 0.5 Mpa, as shown in Figure 22.

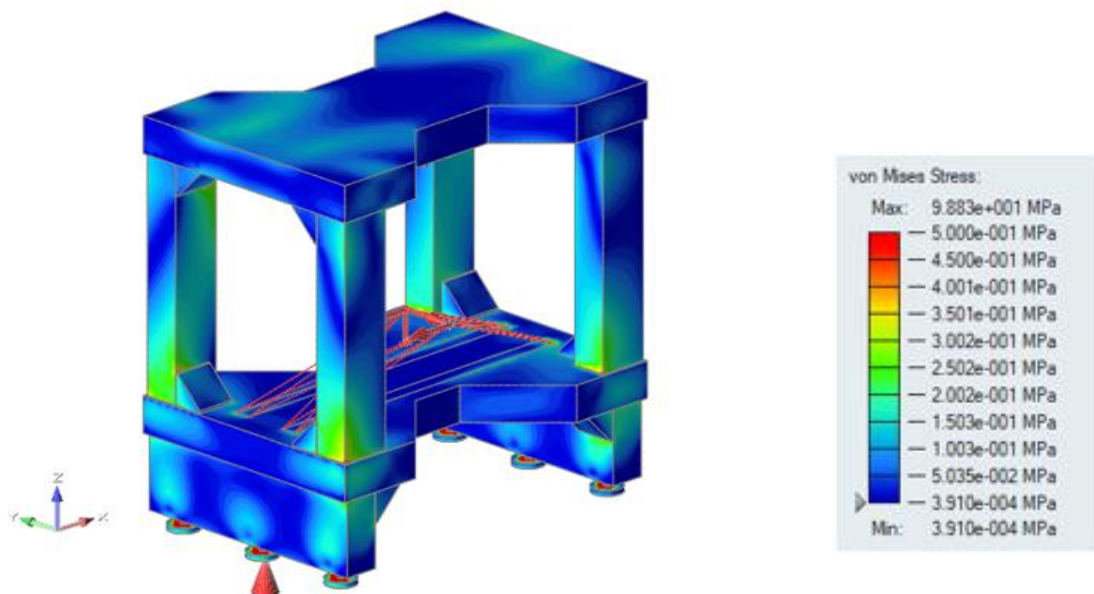


Figure 22 - Re-scaled VM stress contour

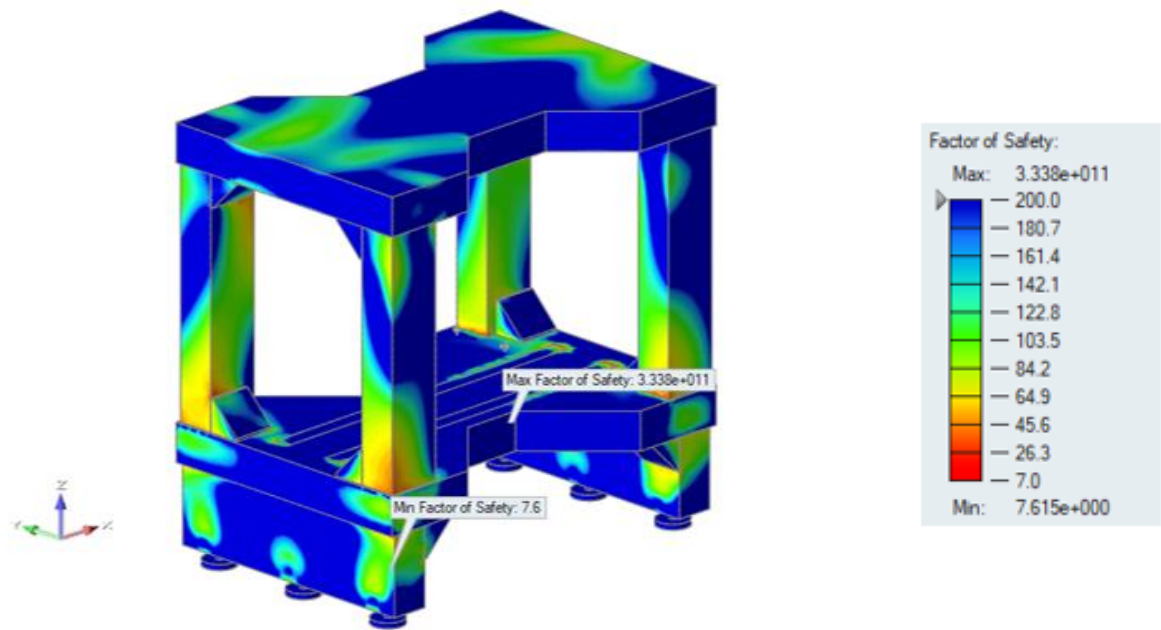


Figure 23 - Factor of safety

As it was done in the case of Von Mises stresses, due to the very big difference in between the maximum and minimum value of the factor of safety (FoS), it was needed to rescale the legend on the right of the image in order to better appreciate the variation of the FoS in different zone of the structure. The most important and remarkable values extrapolated from the static analysis are summarized in Table 4.

Mechanical performances of the original structure			
Mass [Kg]	Maximum resultant displacement [μm]	Maximum Von Mises stress [Mpa]	Minimum factor of safety
1423.6	13.95	98.8	7.6

Table 4 - Mechanical performances of the original structure

By looking to this table and considering what is the ultimate goal of this study, namely the reduction of the mass of the structure without deteriorating its mechanical performances, especially in terms of displacement, it is possible to notice that there could be room for improvement. In fact, the highest tensions are concentrated in quite small areas in which the factor of safety has a huge margin from the value that can be considered critical.

5. Topology optimization process

The topology optimization process allows finding, given a defined design domain, the best distribution of the material, in order to meet a series of performance targets for a predefined set of loads and boundary conditions [8]. This process can be subdivided into mainly five phases:

- Phase 1: Design and non-design space definition
- Phase 2: Set-up of the optimization's parameters
- Phase 3: Analysis of the optimized design
- Phase 4: Re-construction of the optimized model
- Phase 5: Analysis of optimized model

5.1. Design and Non-Design space definition

Since the topology optimization process starts at the design concept level it is important to clarify which is the volume occupied by the device, also called packaging space, and which part of it can be chosen to perform the optimization. For this reason, the software utilized for the optimization process requires the distinction between a design and a non-design space, giving in such a way, the right input parameters to the algorithm.

5.1.1. Non-design space

The non-design space (NDS) is that region of the packaging space which has not to be modified during the optimization process, whose geometrical feature cannot be changed and whose mass cannot be redistributed or removed from the optimization algorithm. Typically are non-design space the zones of connections and/or interference with other elements, or regions that have to exist for functional reasons. Non-design space also has an important role from the numerical point of view, in fact, it is recommended to apply loads and supports to it, and not directly to the design space, avoiding looming over meaningless results.

As regards the structure under analysis, the non-design space was defined considering the functionality of the top and bottom plate, which have to support the guideways mounted on it in order to allow the motion of axes in the X-Y plane, and the space occupied by those axes due to their own length and the stroke allowed over the guideways.

5.1.2. Design space

The design space (DS) is defined as the part of the packaging space that is the object of the optimization process, in other words, is the volume in which the mass is distributed in order to reach the target of the optimization, considering the loading and constraining conditions. Ideally, the best design space would be the entire packaging space as it has the greatest potential to return the optimal concept design [8]. Unfortunately, this is not always possible, because there are some issues that have to be taken into account during the design space definition, such as human and/or instrument accessibility during maintenance services or during the system's working cycle.

During the development of this thesis, due to the feedback given by the results obtained at the very first attempts, and in order to get the best outcome possible, it was necessary to change the approach on the definition of design and non-design space. This kind of evolution is illustrated in the following pages, starting from the simplest model possible, with very few design constraint, until the last one, which gives the final reproducible result.

For the purpose of clarity, in the figures from now on encountered, the distinction between DS and NDS is made by using two different colours, reddish-brown for design space and grey for the non-design space.

5.1.3. Model 1 – Full re-design

The first model used to perform the optimization, as shown in the figures below, was thought in order to give the algorithm the highest level of freedom possible, avoiding any kind of constraint, just to understand which really are the loading paths on the design space and in order to understand if it would have been possible to get to a full re-design of the structure.

Figure 24 shows the non-design space for this model, which consist only on two plates 20 mm thick that define a sort of support for the guideways where the loads are applied and the two 20 mm thick slabs, which define the portion of the structure in contact with the ground. The material selected for the non-design space is granite, in order to guarantee the thermal stability and flatness required in this zone. The void in between the two grey granite planes can as well be considered as a non-design space because it is the zone in which the axes moves, which means that no structural part can be located in there.

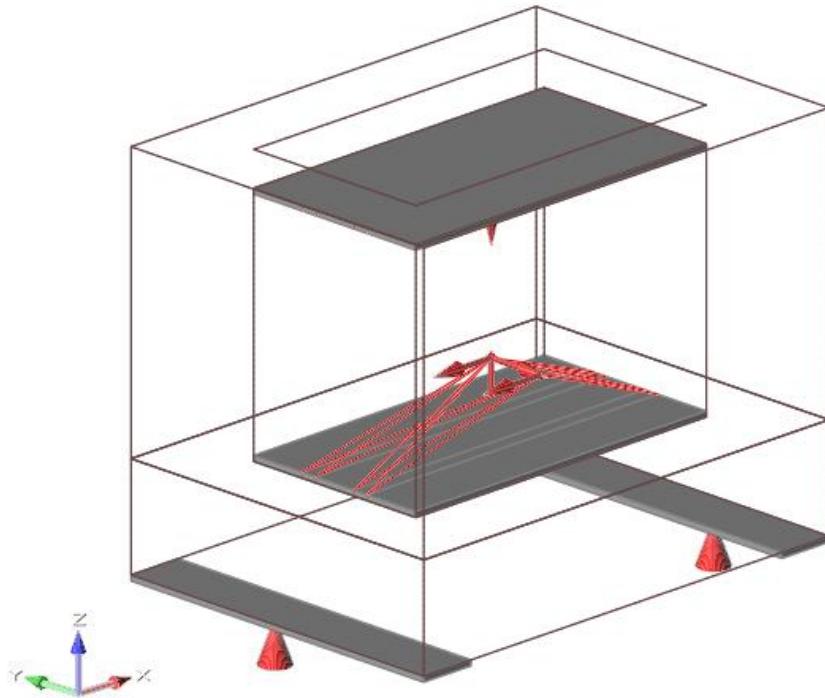


Figure 24 – Model 1 – Non-design space

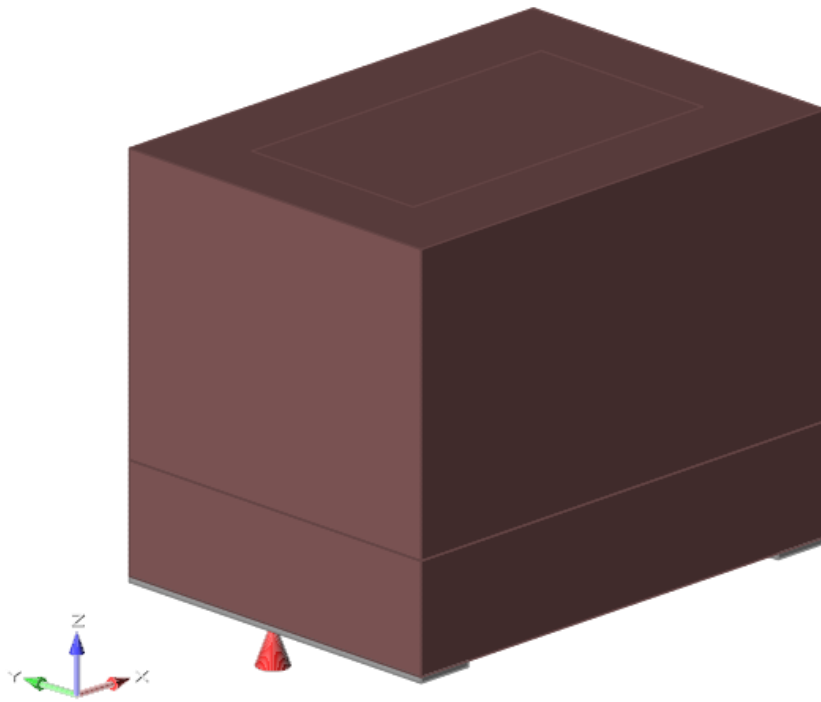


Figure 25 – Model 1 – Design space – Isometric view

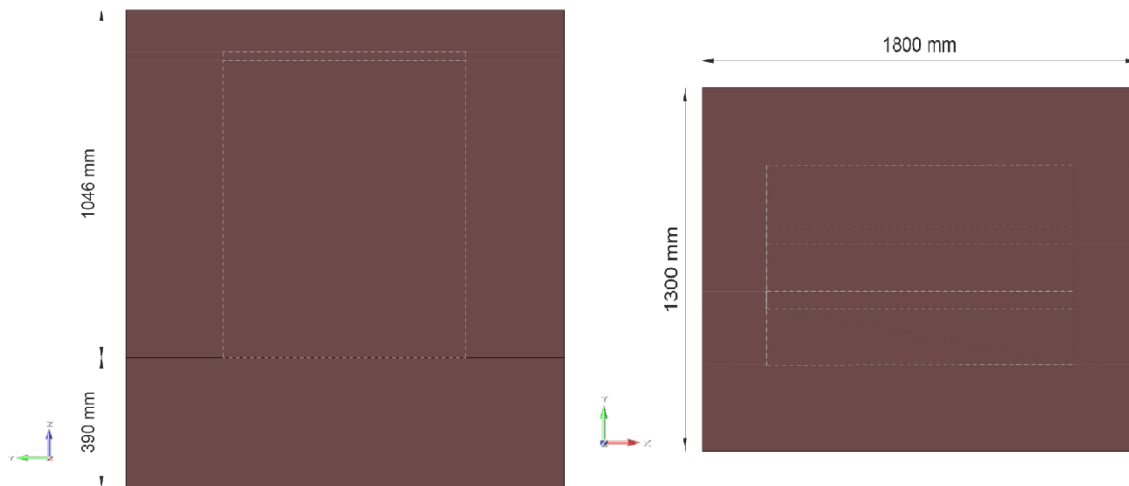


Figure 26 - Model 1 - Design space - Orthogonal views

Figures 25 and 26 instead show in red what is defined as design space, and as mentioned before, it represents all the available space in order to re-distribute the mass in the best way. It can be divided into two parts: the upper one is more or less like a shell which embraces the top and bottom planes, and the lower one, which represents the support of the upper part and the connection to the ground. The outer dimensions of the model overcome the ones of the original structure, which means now there is a lot more volume available just because there was the necessity to understand if and where the material is needed to be placed. The material defined for the design space is Aluminum 6061-T6, available in the material library of the software, and selected due to the higher mechanical properties with respect to the granite.

Granite vs. Aluminum 6061- T6				
Material	Young's modulus [MPa]	Density [kg/mm ³]	Yield stress [MPa]	Coefficient of Thermal expansion [mm/mm · K]
Granite	50000	2.63 x 10 ⁻⁶	14.6	6.5 x 10 ⁻⁶
Aluminium 6061-T6	75000	2.7 x 10 ⁻⁶	241.3	23.5 x 10 ⁻⁶

Table 5 - Comparison between Granite and Aluminum 6061-T6

As we can notice from Table 5, even if the aluminium's density value is slightly higher than the granite's one, it presents much higher mechanical properties such as the Yield stress and especially Young's modulus, which means that with a lower amount of mass a stiffer structure can be obtained. Another parameter to take into better consideration during this process is the coefficient of thermal expansion, which describe how the dimension of

an object changes with a variation of temperature. The granite is characterized by a very low thermal expansion coefficient, almost four times lower than the aluminium's one, which means that, for the same thermal gradient, the granite structure undergoes to a deformation four times lower than the one made in aluminium, avoiding losses of stability and precision during the testing process.

5.1.4. Model 2 – Inspection window

As already mentioned, it is not always possible to give the highest grade of freedom to the design space when performing an optimization, in fact, from the analysis of the results of the optimization on the first model, has emerged the need to have a window in the front and rear side of the system due to the following reasons:

- Mounting of the axes and all the related instrument on top of the guideways
- Mounting of the board's conveyor system
- Accessibility during maintenance and inspection
- Visibility of the testing area

Figure 26 depicts the design and non-design space of model 2, and as it is possible to notice, the non-design space is identical to the one of model 1. The only thing changing is the design space, which now presents a window on both the front and rear side of the model having dimensions 700 mm x 1200 mm as represented in Figure 27.

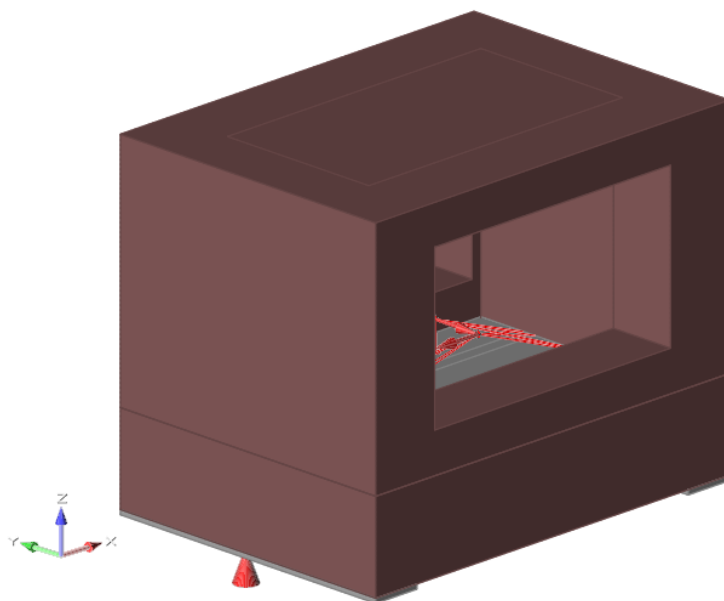


Figure 27 - Model 2 – Inspection window

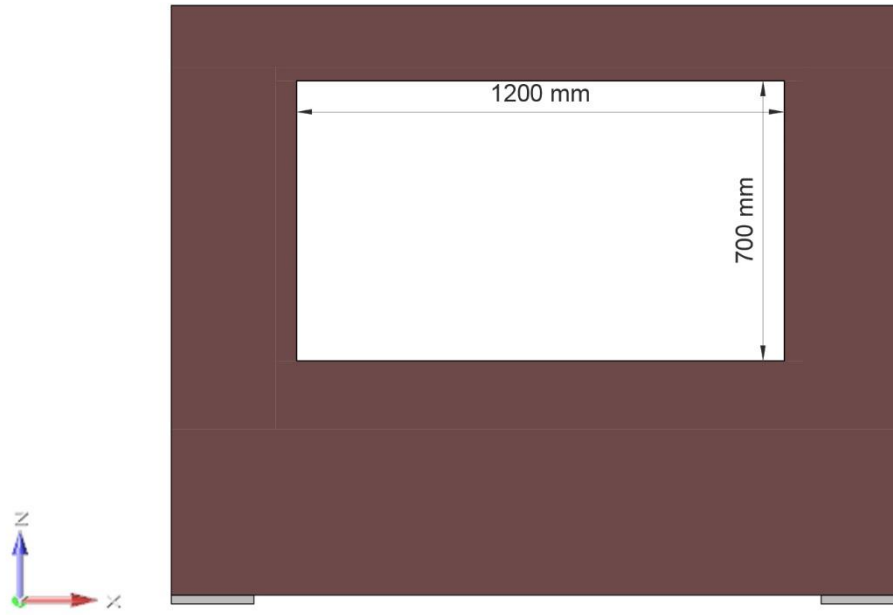


Figure 28 – Model 2 - Window's dimension

As already mentioned in chapter 4.1, the overall structure can be divided into two parts: the main cell and its support base. From the analysis of the results obtained from the first two models' optimization, and due to the difficulties in finding an actual solution able to reproduce the optimized design, it was needed to re-think the optimization process dividing it into three steps:

- Performing the optimization analysis for the main cell only
- Reconstruction of the cell's optimized design
- Optimization of the support base jointed with the optimized cell

5.1.5. Model 3 – Main cell

The main cell is the part of the structure that encloses all the devices that move, hold the boards and perform the testing operations, so it was relevant to find a solution that maximizes its stiffness in order to reduce at minimum the relative displacement between its constituent parts.

The model proposed, shown in Figure 28, is the outcome of several hypothetical proposals and is the one that gives back reasonable results, exploitable as a starting point for the realization of the real structure.

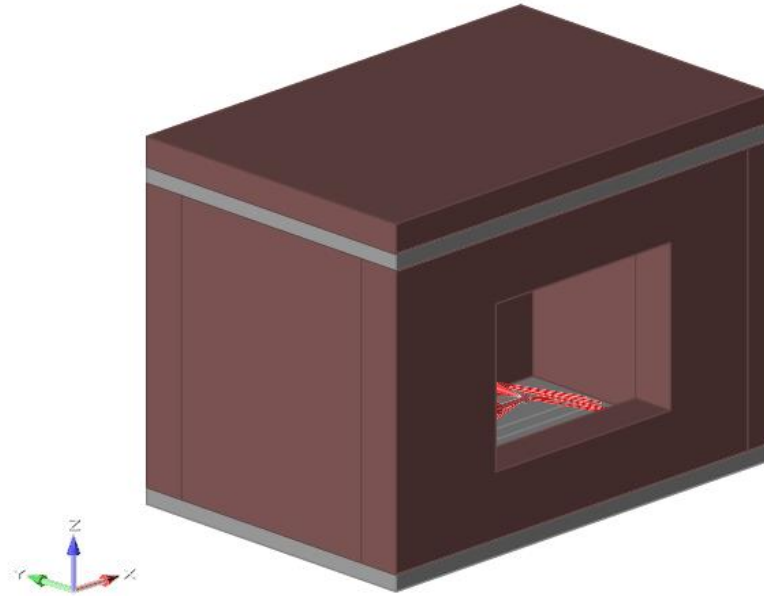


Figure 29 – Model 3 - Main cell

As can be seen, the non-design space, depicted by the two grey planes, is meant to represent the guideways' support planes; its dimensions are shown in Figure 29 and the material assigned to it is the granite. The 50 mm thickness of each plate was chosen as a threshold value in order to understand if it would have been enough to bear the loads applied without increasing far too much the stresses causing the collapse of it.

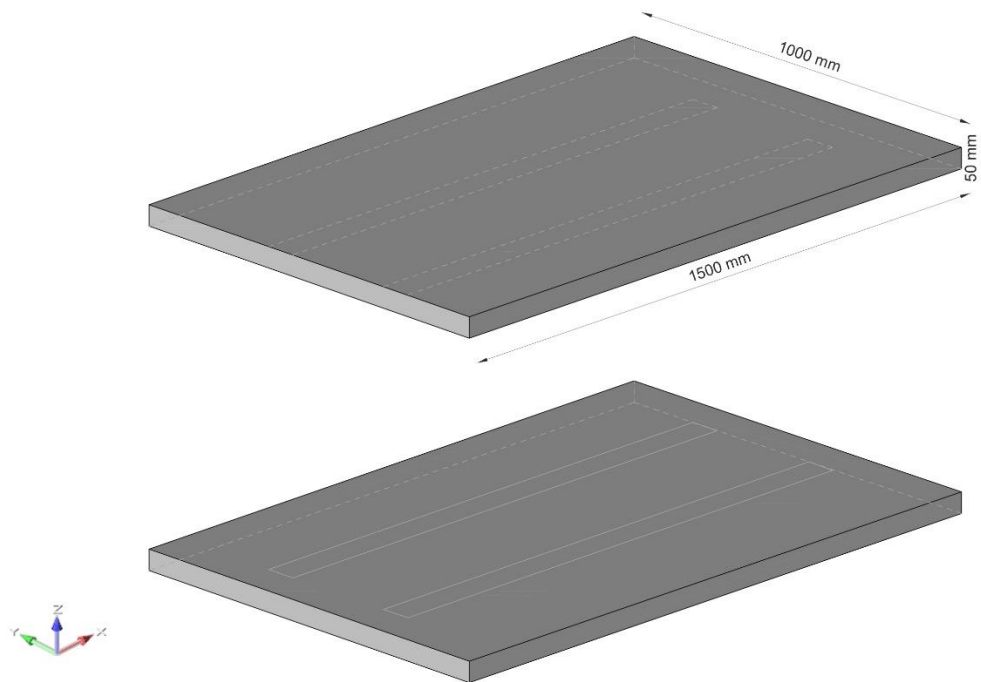


Figure 30 - Model 3 - Non-design space

The design space is also made of two parts; the one over the upper plate of the non-design space was placed to verify if any further amount of mass is required on top of the guideways in order to sustain the loads applied. The second one instead represents all the available space that can be used to connect the top and bottom granite plates. Just like the model 2, also this model is provided with a central window on the front and rear walls, having the same utility but different dimensions. The design space of model 3 and the window's dimensions are represented respectively in Figure 30 and 31.

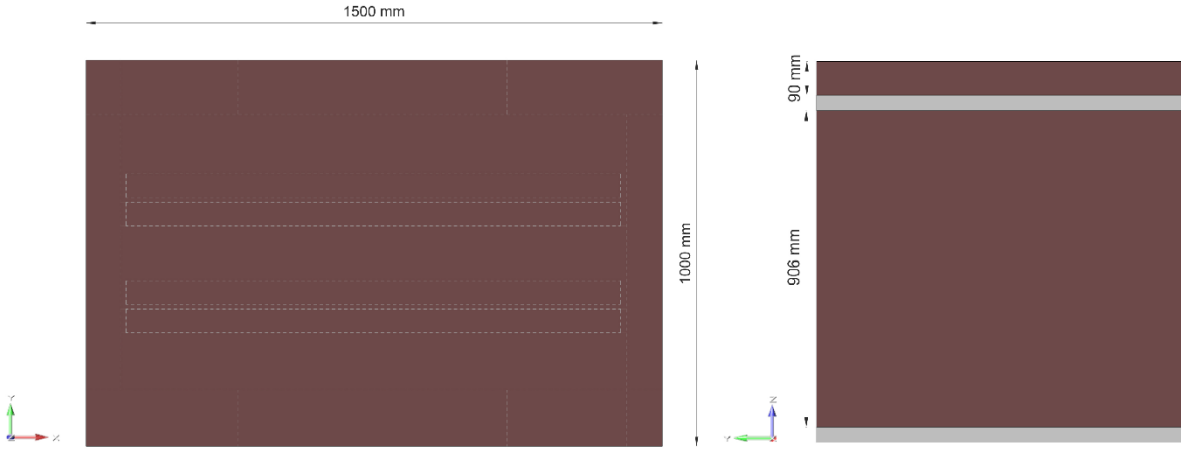


Figure 31 - Model 3 - Orthogonal views

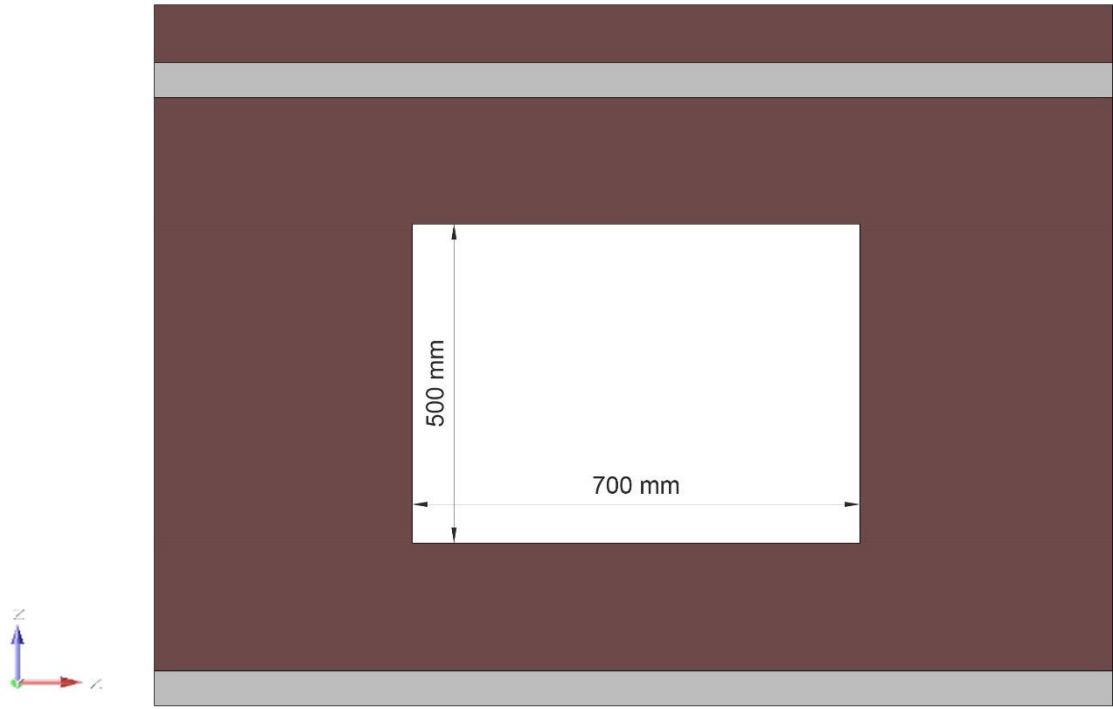


Figure 32 - Model 3 - Window's dimensions

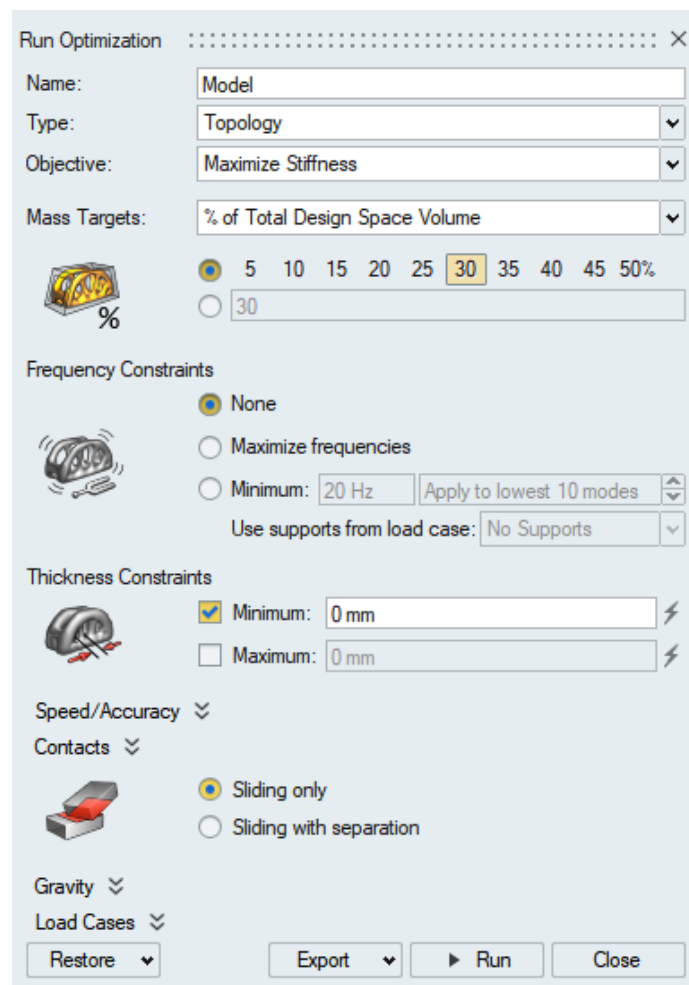
5.2. Set-up of the optimization's parameters

As already mentioned in chapter 3.2, any optimization problem is characterized by an objective function related to some design variables and constraints. Solidthink Inspire allows choosing between three different objectives:

- Maximize stiffness
- Maximize frequency
- Minimize mass

where only the first and the last are the ones often used for topology optimization.

Maximizing the stiffness (or minimizing the compliance) of a design space allows obtaining a material distribution which will ensure the lowest amount of displacement of the model under the action of the applied loads. This is a good choice in order to discover the load path in the model.



The screenshot shows the 'Run Optimization' dialog box with the following settings:

- Name: Model
- Type: Topology
- Objective: Maximize Stiffness
- Mass Targets: % of Total Design Space Volume
- Mass Targets: 30 (selected)
- Frequency Constraints: None
- Thickness Constraints: Minimum: 0 mm (checked), Maximum: 0 mm
- Speed/Accuracy: (collapsed)
- Contacts: (collapsed)
- Sliding: Sliding only (selected)
- Gravity: (collapsed)
- Load Cases: (collapsed)
- Buttons: Restore, Export, Run, Close

Figure 33 – Stiffness maximization parameters

As shown in Figure 24, by choosing to maximize stiffness as objective, it is necessary to choose one or more of the following constraints:

- Mass targets: it used to define the quantity of mass to be preserved which can be indicated as a percentage of total design space volume, or can be specified individually for each design space.
- Frequency constraints: in this case, it is possible to choose if to maximize the frequency and the stiffness at the same time, or to set a minimum frequency value the optimized model should present, for example, to avoid resonance problems.
- Thickness constraints: allows controlling the size of the element in the proposed geometry by specifying a maximum and/or minimum thickness. This parameter affects the computational time of the algorithm.

By choosing the mass minimization, the algorithm proposes the lightest design possible that can still support the applied loads. As in the previous case, when choosing this objective it is recommended to set a stress constraint in order to limit the maximum stress in the model, by imposing a minimum safety factor, as shown in Figure 25.

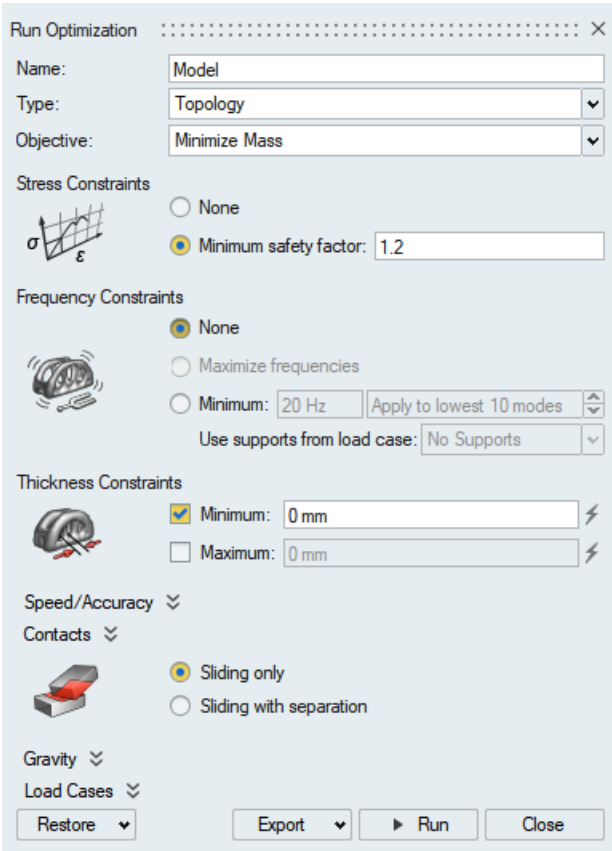


Figure 34 - Mass minimization parameters

6. Results

This chapter is dedicated to the presentation of the results of the process of topology optimization of the models exposed in the previous chapter.

6.1. Iso-density curves results' interpretation

Once the process of optimization is ended, Inspire allows analyzing the results through the shape explorer (Figure 34), by using the iso-density curves interpretation method. It consists of the definition of a density cut-off value upon which is drawn an iso-density curve which describes the contour of the resultant topology. The shape explorer thanks to the topology slider allow setting this cut-off value, deleting all the elements with a lower density value and promoting to the unit value all the other elements.

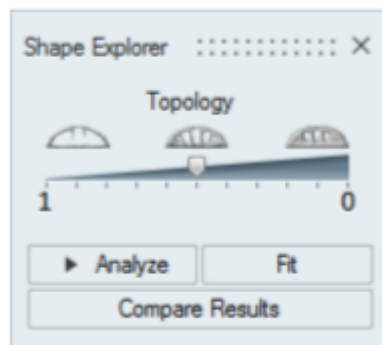


Figure 35 - Shape explorer

This tool was used in order to understand how, by varying the cut-off value, the shape, the mass and consequently the mechanical properties of the optimized model changed, allowing to find a good compromise between the different solutions.

Generally, the optimal result is reached in a point on the slider in order to produce a topology with all the loads and support locations connected, with no separated areas. If by moving the slider, the optimized shape doesn't change excessively, it means that a good solution has been reached and it is possible to define new, more restraining design targets.

6.2. Model 1

In Figure 35 it is possible to appreciate the optimized shape of model 1 at three different cut-off values: 0.8, 0.2 and 0.3. As can be seen, there is a slight difference in between the three models, mainly observable on the walls in the upper part of the structure, which means that for this design space the optimal solution has been reached. Figure 36 instead shows the deformed shape and the maximum resultant displacement indication for the 0.5 cut – off value's shape. By analysing the optimized shape it seems that there is no need for further mass above the top plane and that this kind of X-shaped supporting frame allows bearing the acting loads, further support instead is needed in the central zone of the bottom plane, just in the guideways direction.

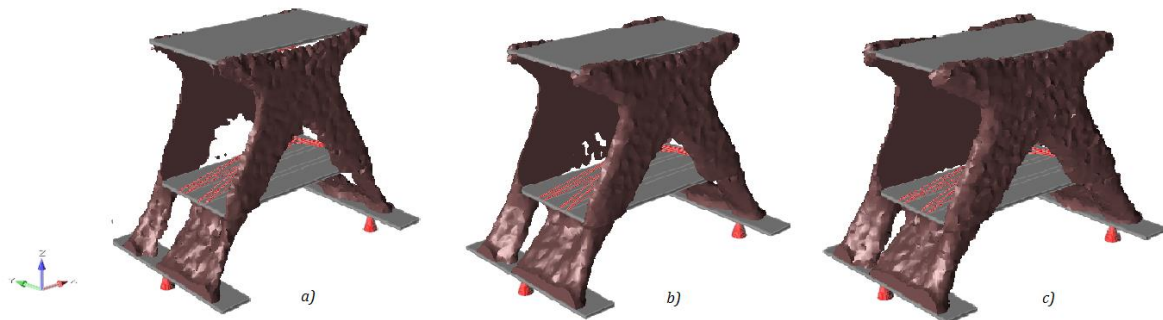


Figure 36 - Optimized shape for different cut-off values: a) 0.8; b) 0.5; c) 0.3

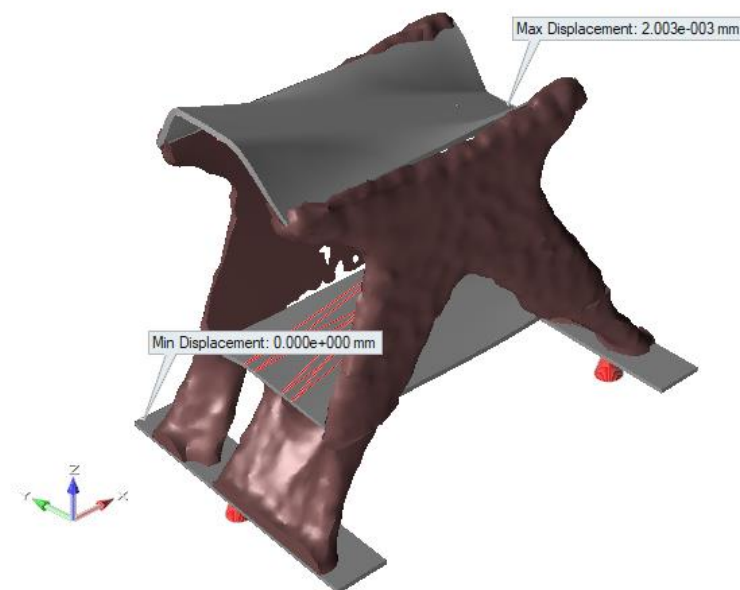


Figure 37 - Model 1 - 0.5 cut-off value - Deformed shape

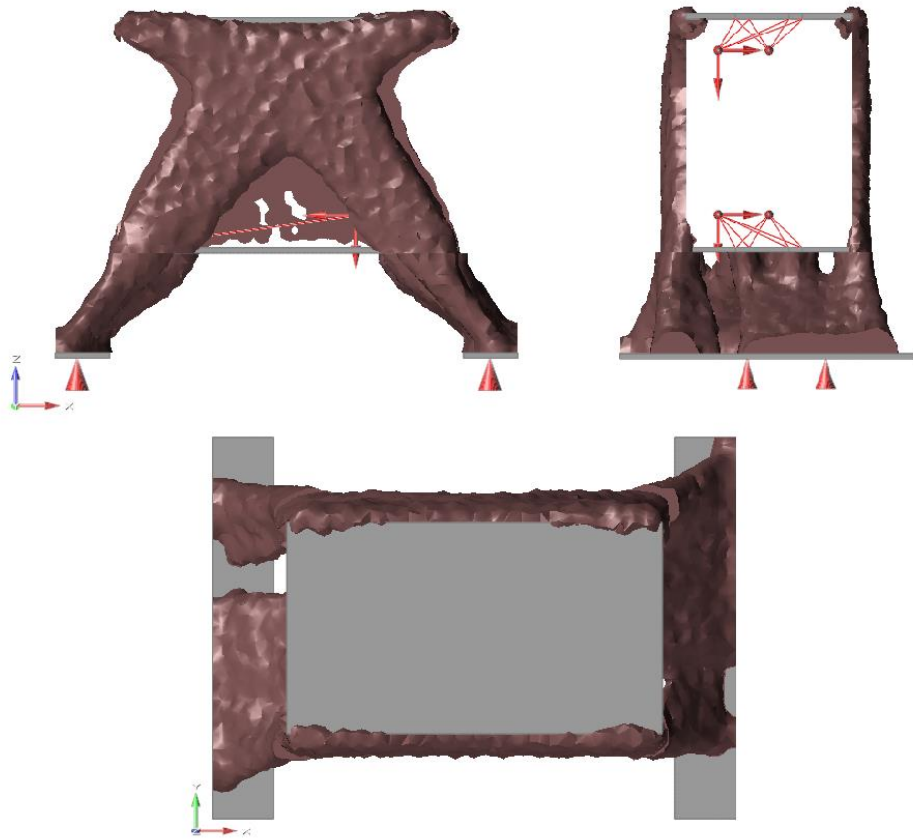


Figure 38 - Model 1 - 0.5 cut-off value - Orthogonal views

Model 1			
Cut-off value	0.8	0.5	0.3
Mass [kg]	532.12	740.58	891.96
Max Displacement [μm]	2.82	2	1.62

Table 6 - Models' comparison for different cut-off values

From Table 6, which lists the mass and maximum resultant displacement values for the three different shapes, it is possible to make some considerations: for each one of the shapes, a considerable mass reduction and an outstanding improvement in performances is achieved with respect to the original model, but on the other hand, it is not so easy to find a solution to actually reproduce a geometry of such type with conventional manufacturing technologies and moreover, the absence of the central window required as a design constraint makes this solution not adequate to the final purpose.

6.3. Model 2

In the following figures are presented the three different shapes produced by the optimization processes on model 2. Each figure has been named in such a way to understand the optimization's parameters used for them. All the geometries were subjected to structural static analysis in order to compare their performances with the original one, and some of the most relevant parameters such as the mass, the mass' percentage variation with respect to the original structure, the maximum resultant displacement, the maximum Von Mises stress, the minimum safety factor and finally the chosen density cut-off value were collected in Table 7.

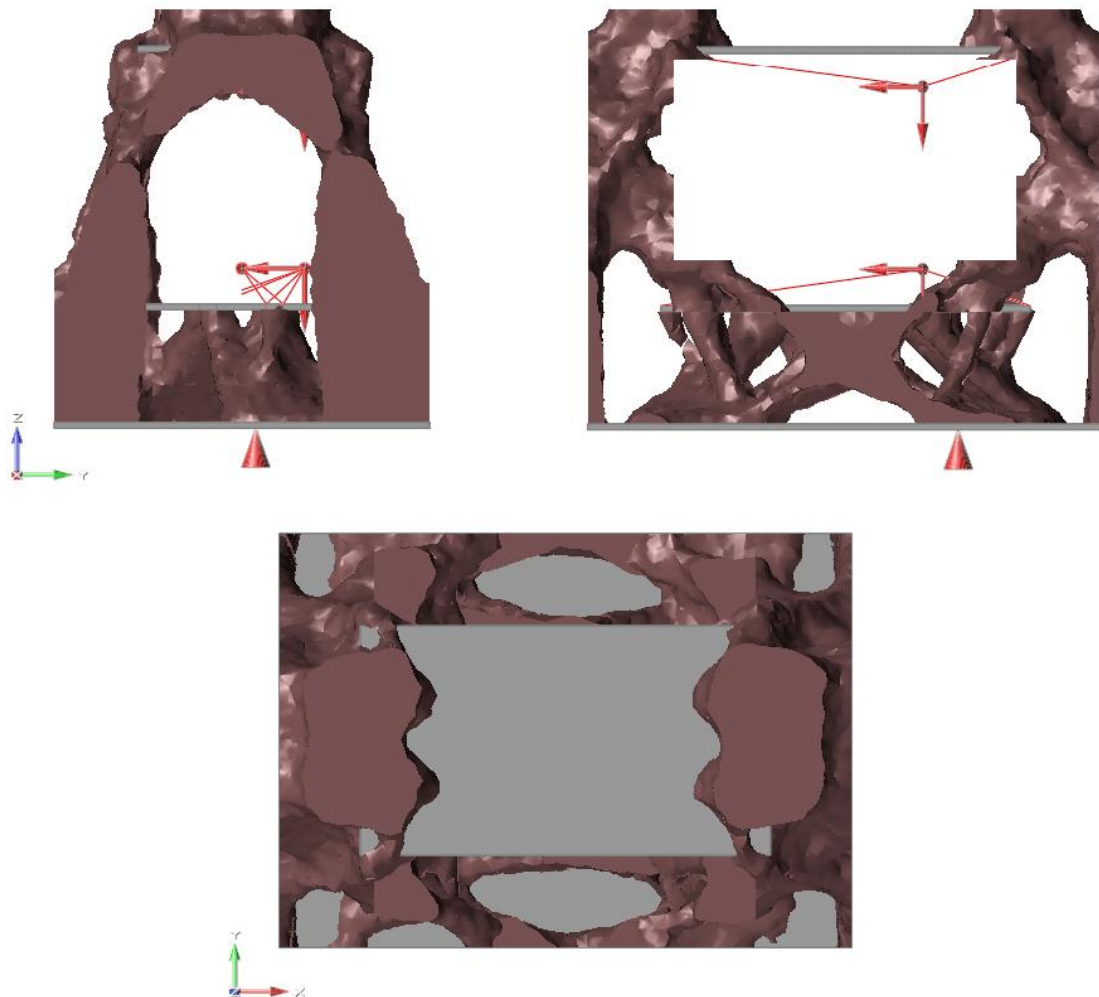


Figure 39- Model 2 - maxstiff20% – Orthogonal views

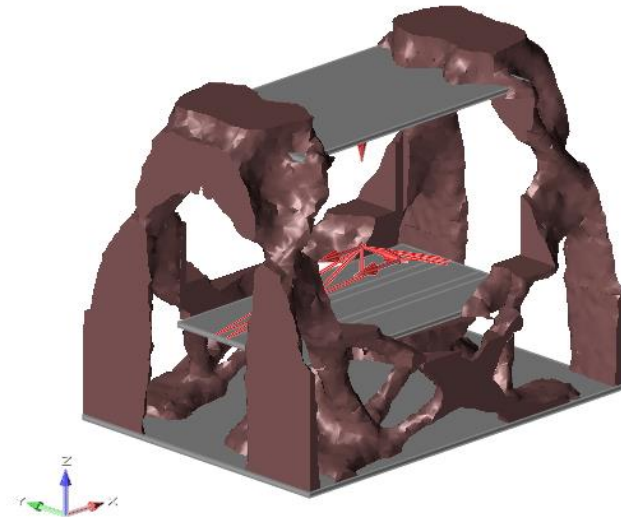


Figure 40 - Model 2 - maxstiff20% - Isometric view

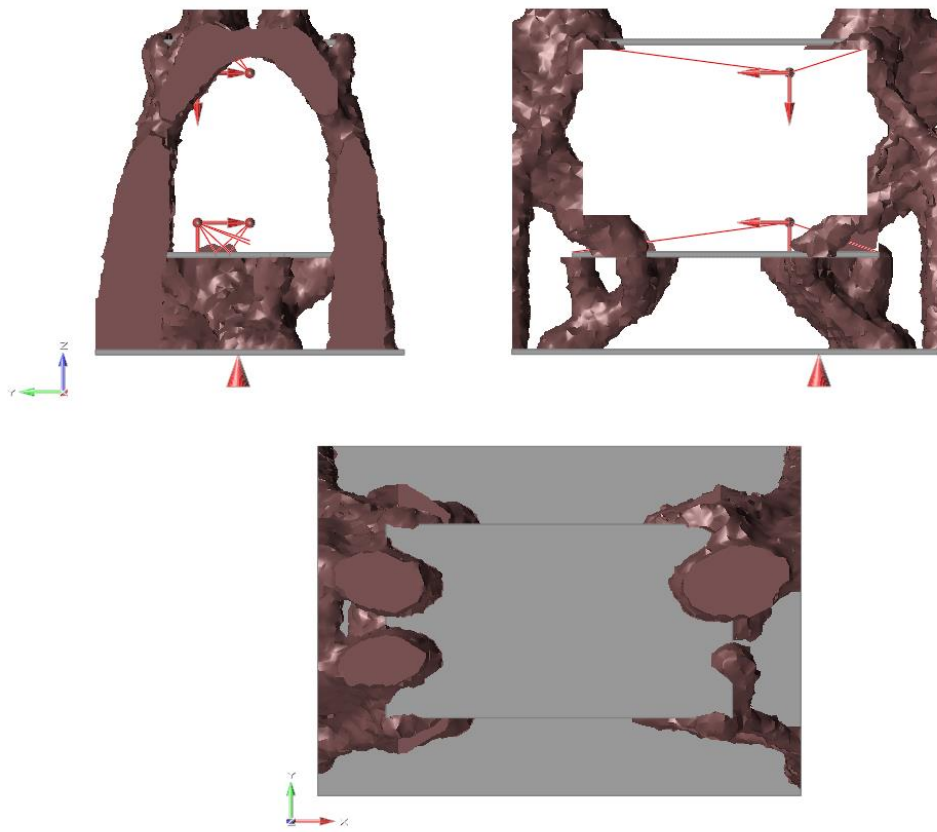


Figure 41 - Model 2 - maxstiff10% - Orthogonal views

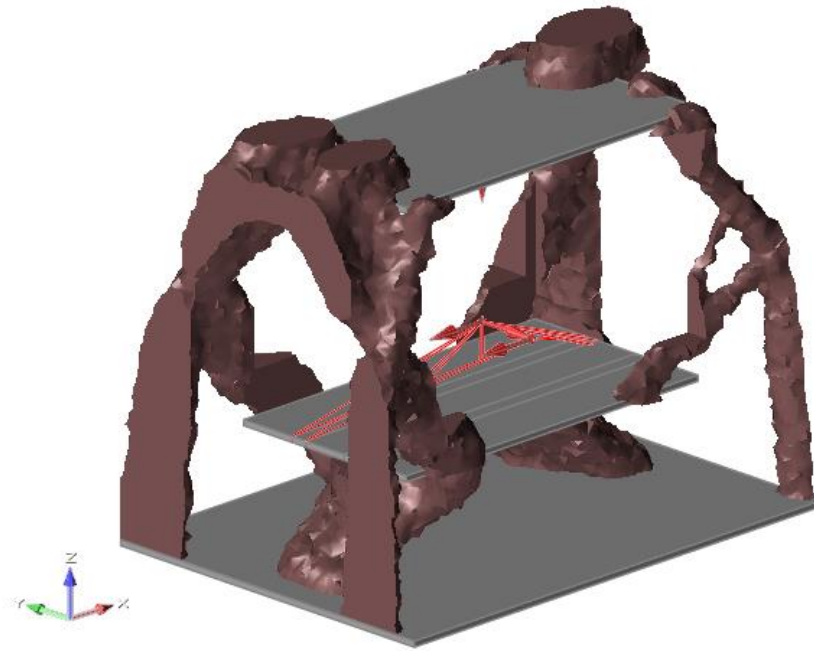


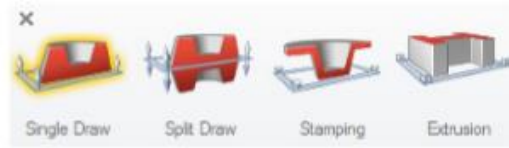
Figure 42 - Model 2 - maxstiff10% - Isometric view

Since the applied loads are asymmetric with respect to the ZX plane, as we can see in Figure 41, the optimization process tends to deposit more material in the zone where there is a higher concentration of loads, often resulting in asymmetric elements in the structure. In order to prevent this kind of problem, SolidThinking Inspire allows setting, regardless of the final objective of the optimization, some geometrical constraints for the design space, the so-called shape controls. These tools, described in Figure 42, act on the shape of the optimized topology by forcing it to assume defined geometric characteristics in order to be more easily reproducible with specified manufacturing processes.

Draw Direction



There are four tools available in the Draw Direction menu:



Single Draw and Split Draw are used for casting.

For Single Draw, the parting plane for the two sides of the mold resides outside of the design space.

For Split Draw, the parting plane resides within the design space.

Stamping is used for stamping rather than casting. The resulting shape will be of uniform thickness.

Extrusion will force the resulting shape to have a constant profile.

Symmetry



There are three tools available in the Symmetry menu:



Symmetric defines up to three planes of symmetry.

Cyclic defines a cyclical pattern with asymmetric sectors.

Cyclic Symmetric defines a cyclical pattern with symmetric sectors.

Figure 43 - Shape controls description [6]

Draw direction are useful when the model has to be produced by means of casting as well as stamping processes, symmetry instead is used if there is the need to generate symmetric or cyclically repeating shapes. For the second model, symmetry shape controls were applied to both the upper and the lower part of the design space, as described in Figure 43.

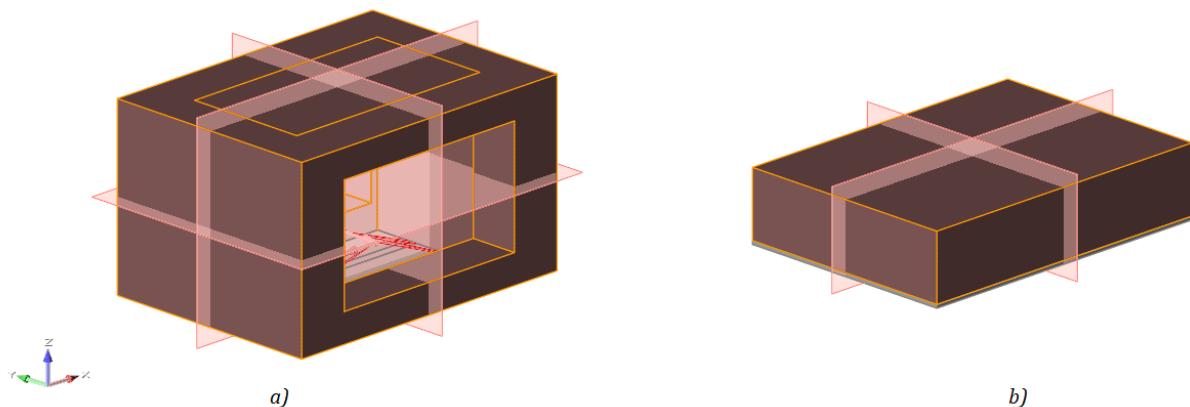


Figure 44 - Symmetry shape control: a) Upper DS (cell); b) Lower DS (support base)

For the upper part of the design space, symmetry planes were applied for each of the three possible directions, for the lower part instead only the ZY and ZX symmetry planes were used.

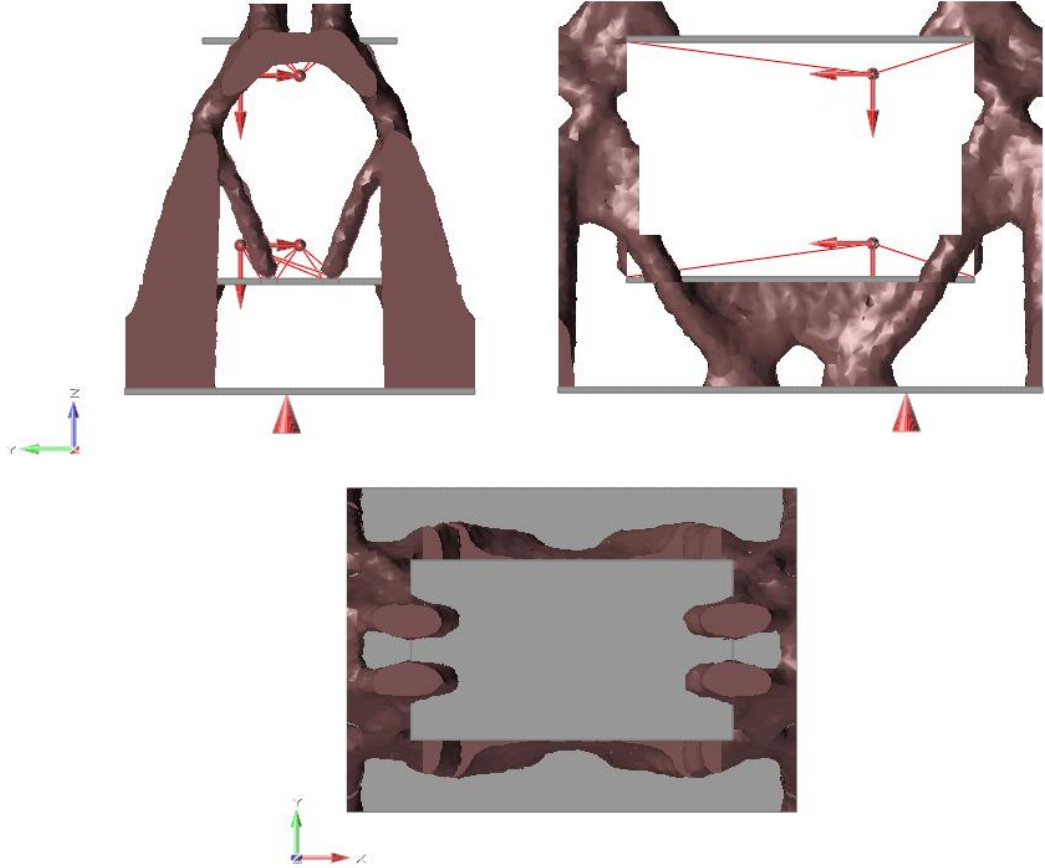


Figure 45 - Model 2 - maxstiff10%_shapecontrol - Orthogonal views

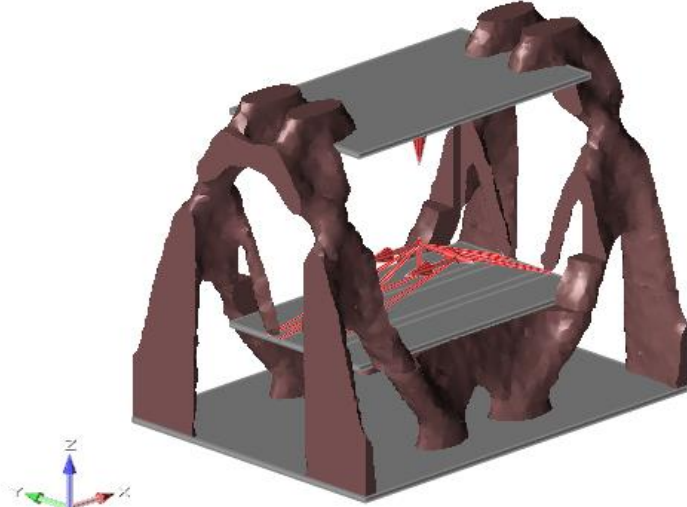


Figure 46 - Model 2 - maxstiff10%_shapecontrol - Isometric view

Mechanical properties of model 2's resultant geometries						
Name	Mass [kg]	DeltaMass%	Max VM stress [MPa]	Max resultant displacement [μm]	Minimum safety factor	Density Cut-off value
maxstiff20%	1030	-27.6	0.46	3.43	122	0.4
maxstiff10%	827.7	-41.9	0.25	5.52	70.3	0.8
maxstiff10%_shapecontrol	690.2	-51.5	0.27	5.02	69	0.5

Table 7 - Mechanical properties of model 2's resultant geometries

By reading to the data present in Table 7 it is possible to understand that by reproducing a structure similar to the one described by the “maxstiff10%_shapecontrol” optimization it is possible to reduce both the mass and the displacement obtaining also a higher factor of safety. There are still few issues that make the production of a similar geometry difficult, such as the connection between the structure and the top plane, and the irregular shape of the four vertical elements that should reproduce the supporting pillars of the entire structure. For this reason, the choice of changing approach to the optimization process was made, giving more relevance to the optimization of the main cell of the structure, thus leading to the third model.

6.4. Model 3

The main cell, due to its functionality, is the most important part of the structure and it should possess the highest possible level of stiffness and geometric stability. The non-design space, made of two 50 mm granite plates, is meant to confer thermal and geometrical stability in the zone of the guideways; instead the design space, made of aluminium due to the higher stiffness to weight ratio with respect to the granite, is meant to assure very low deformation values for a restrained amount of mass. As it was done in the previous pages, the following pictures (from Figure 46 to 54) represent the results of the optimization processes performed on this model, applying to the design space the symmetry shape control in all the cartesian planes.

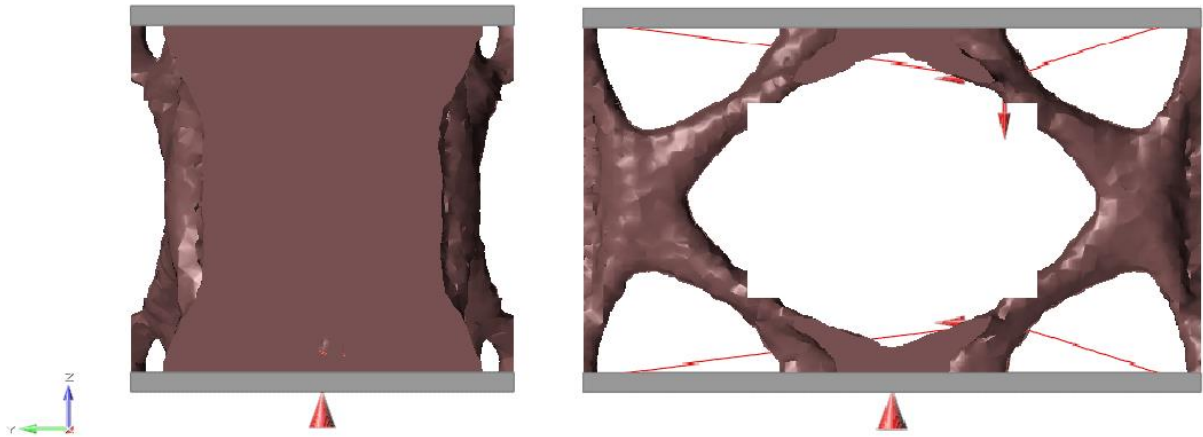


Figure 47 - Model 3 - maxstiff20% - Orthogonal views

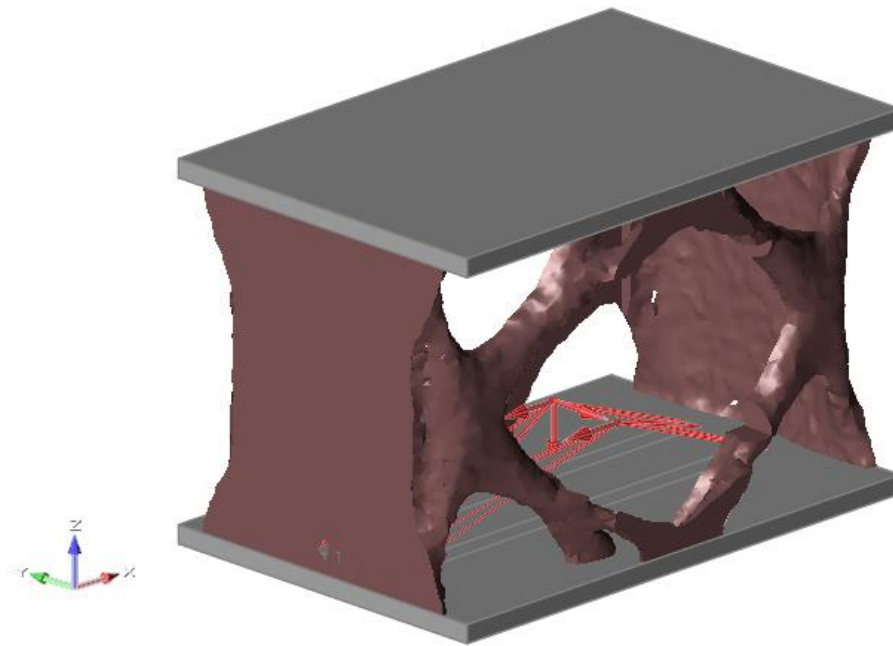


Figure 48 - Model 3 - maxstiff20% - Isometric view

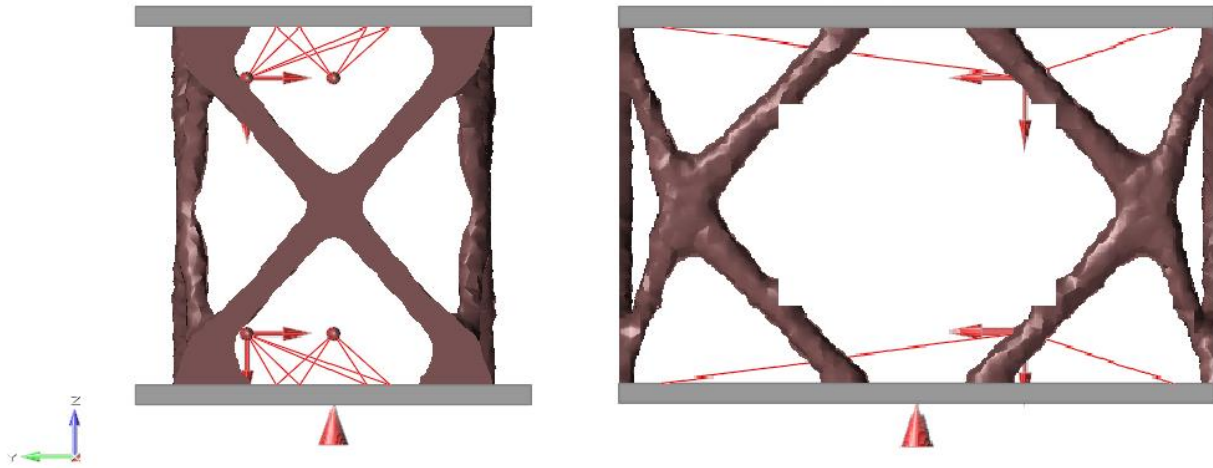


Figure 49 - Model 3 - maxstiff10% - Orthogonal views

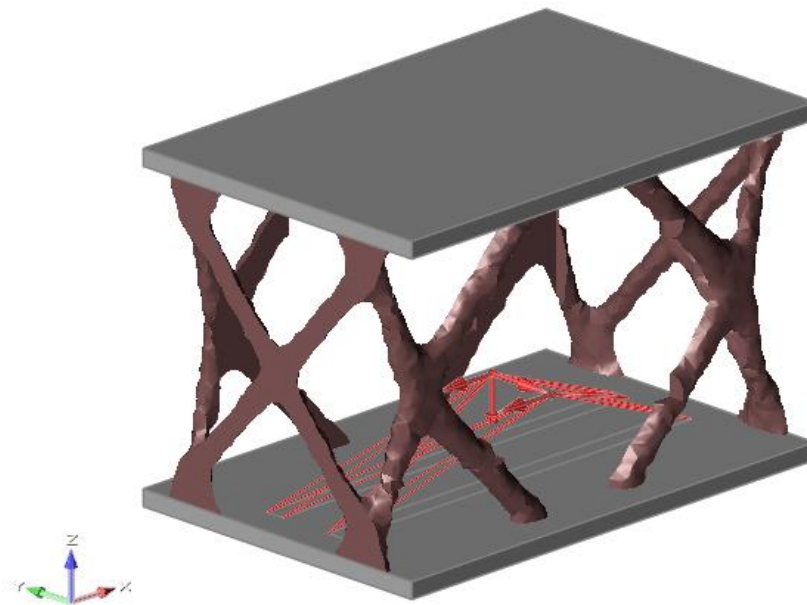


Figure 50 - Model 3 - maxstiff10% - Isometric view

As it can be seen in the last two images, the optimization process results in a sort of reticular support structure which develops along with the load directions, made of slanting elements in the front and rear side and of crossing elements in the right and left side of the structure. The presence of the latter ones is to be considered as an obstruction to the flow of boards due to the possibility for the system to work in a production line thanks to an automatic machine's loading mechanism. For this reason, a further modification to the design space of model 3 was realized which consist of a window on the right and left side, whose shape and dimensions are represented in Figure 50.

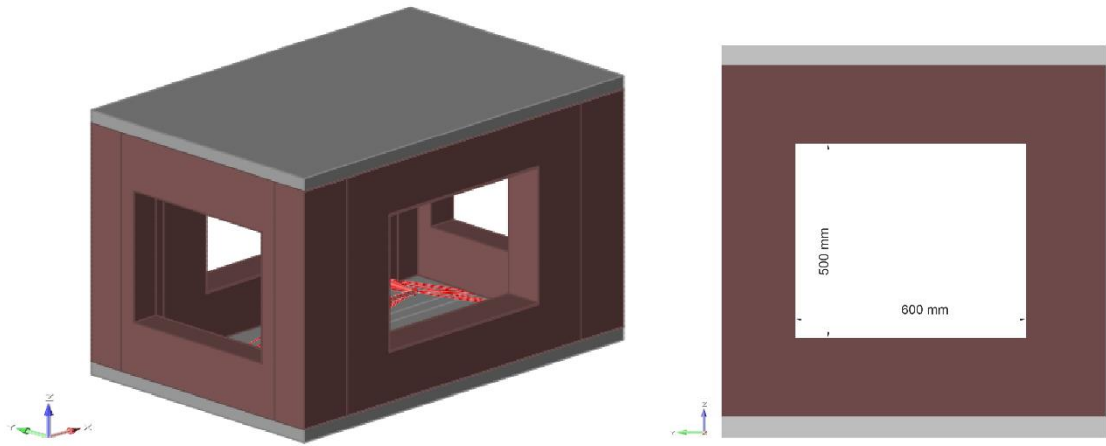


Figure 51 - Model 3.1 - Design space - Window's dimension

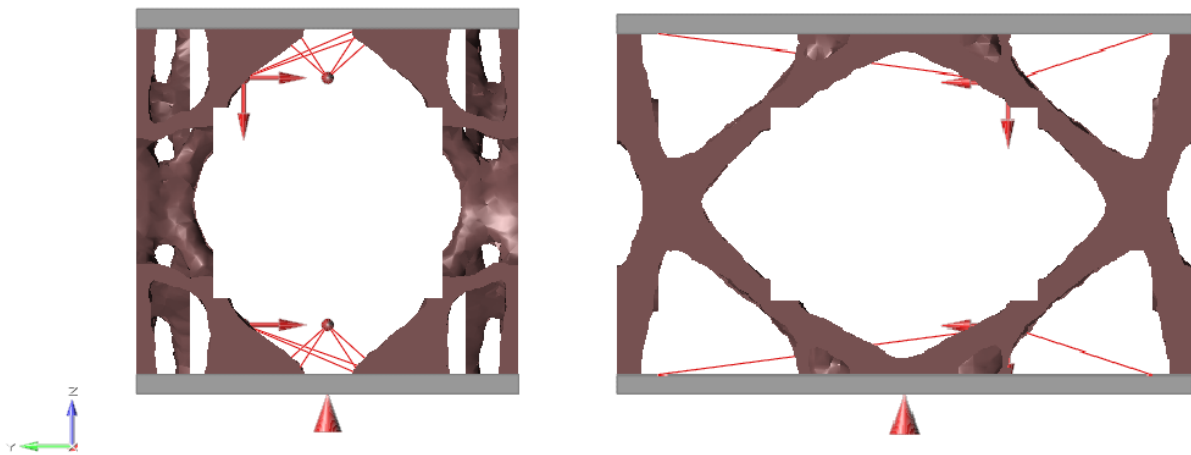


Figure 52 - Model 3.1 - maxstiff20% - Orthogonal views

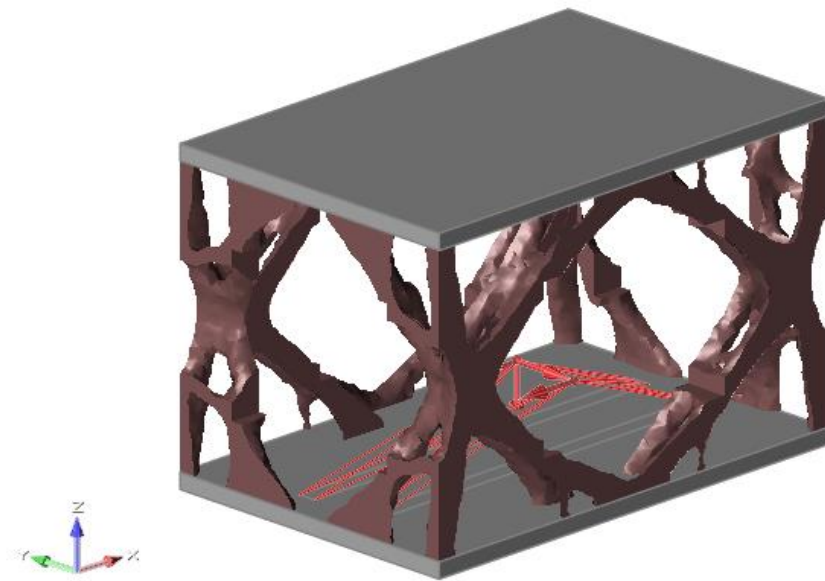


Figure 53 - Model 3.1 - maxstiff20% - Isometric view

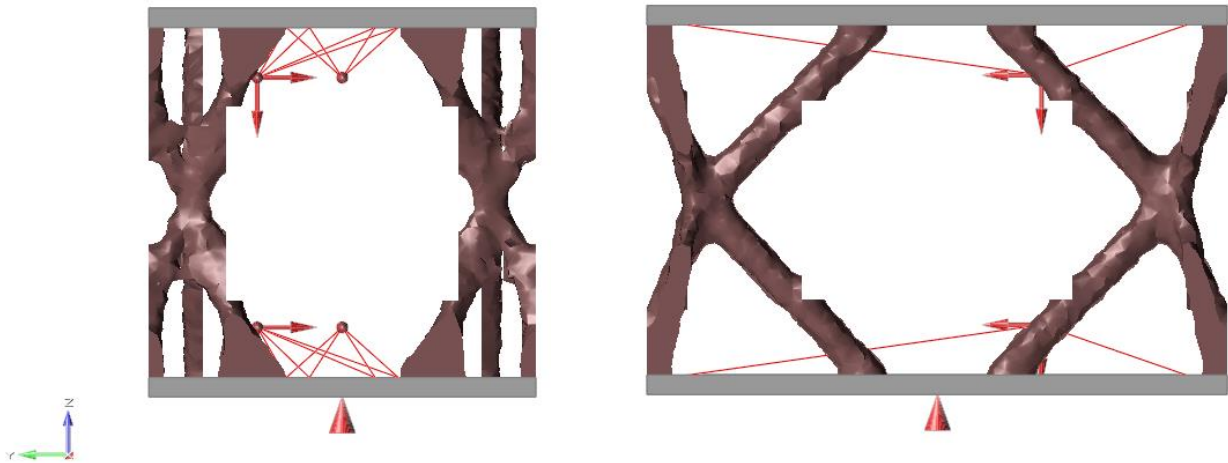


Figure 54 - Model 3.1 - maxstiff10% - Orthogonal views

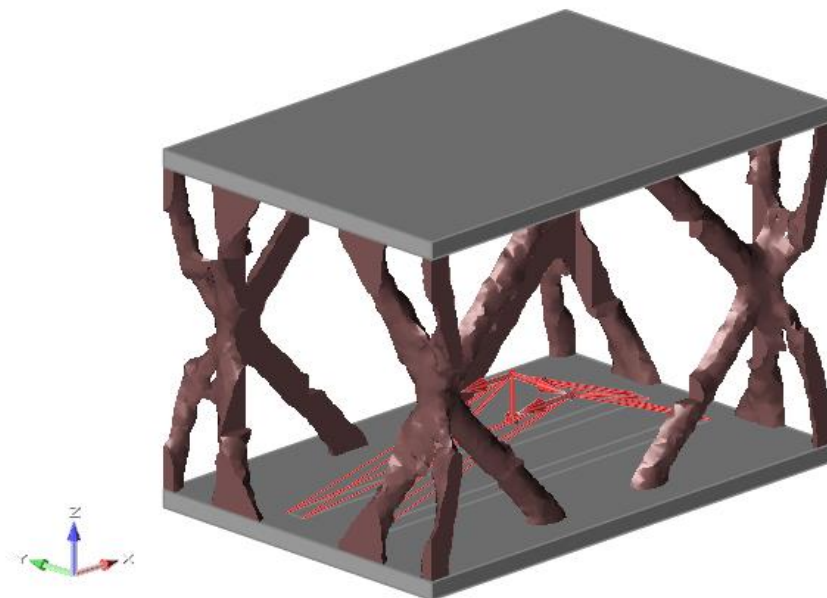


Figure 55 - Model 3.1 - maxstiff10% - Isometric view

Come to the end of this series of optimization, by means of an analysis of the design obtained, it is possible to make few considerations:

- In each of the shape obtained there is the presence of some tilted elements which connect the top and bottom planes with the vertical elements, that in the original model were represented by the pillars.
- These tilted elements appear both along with the X and Y directions, which are the most affected from the acting loads and where it is possible to observe the highest values of deformation.

The next step consists of modelling one or more of the geometries obtained and perform the optimization process for the other part of the structure, the support base. In order to accomplish this task, PolyNURBS, another very interesting tool included in SolidThinking Inspire software was used. PolyNURBS allows creating a solid and continuous free-form geometry directly over the optimized topology. In this case, model 3.1 was taken as a starting point to rebuild the geometry and then connected to the support base's design space, having dimension recalled in Figure 57, for which the symmetry shape control for ZX and ZY planes were applied.

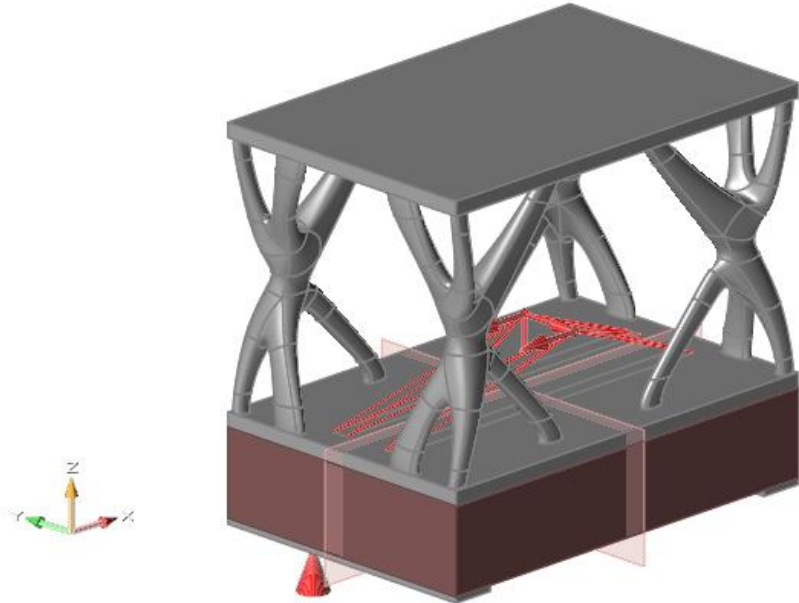


Figure 56 - Support base optimization

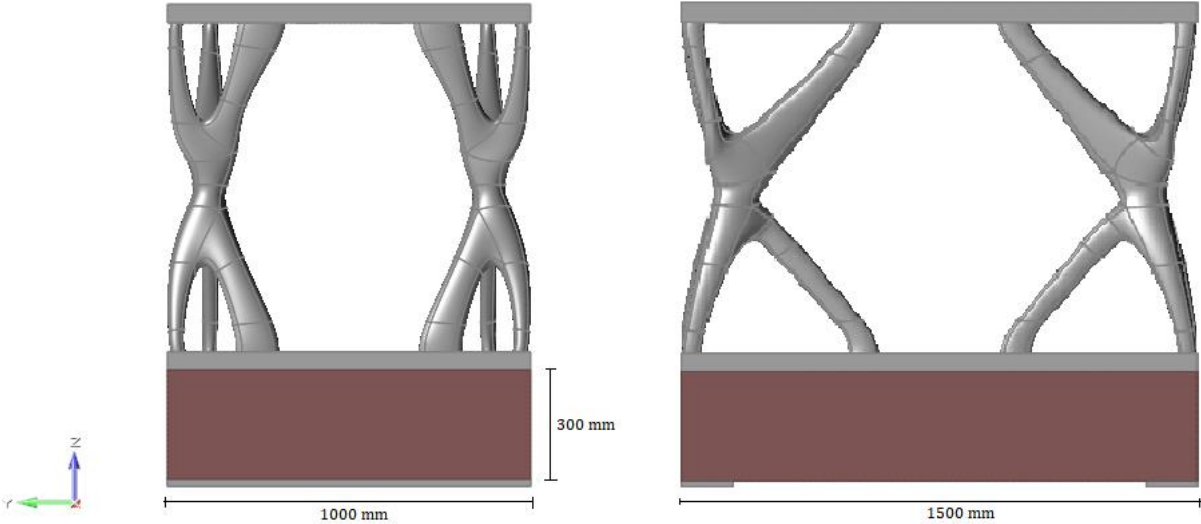


Figure 57 - Support base optimization - Design space's dimensions

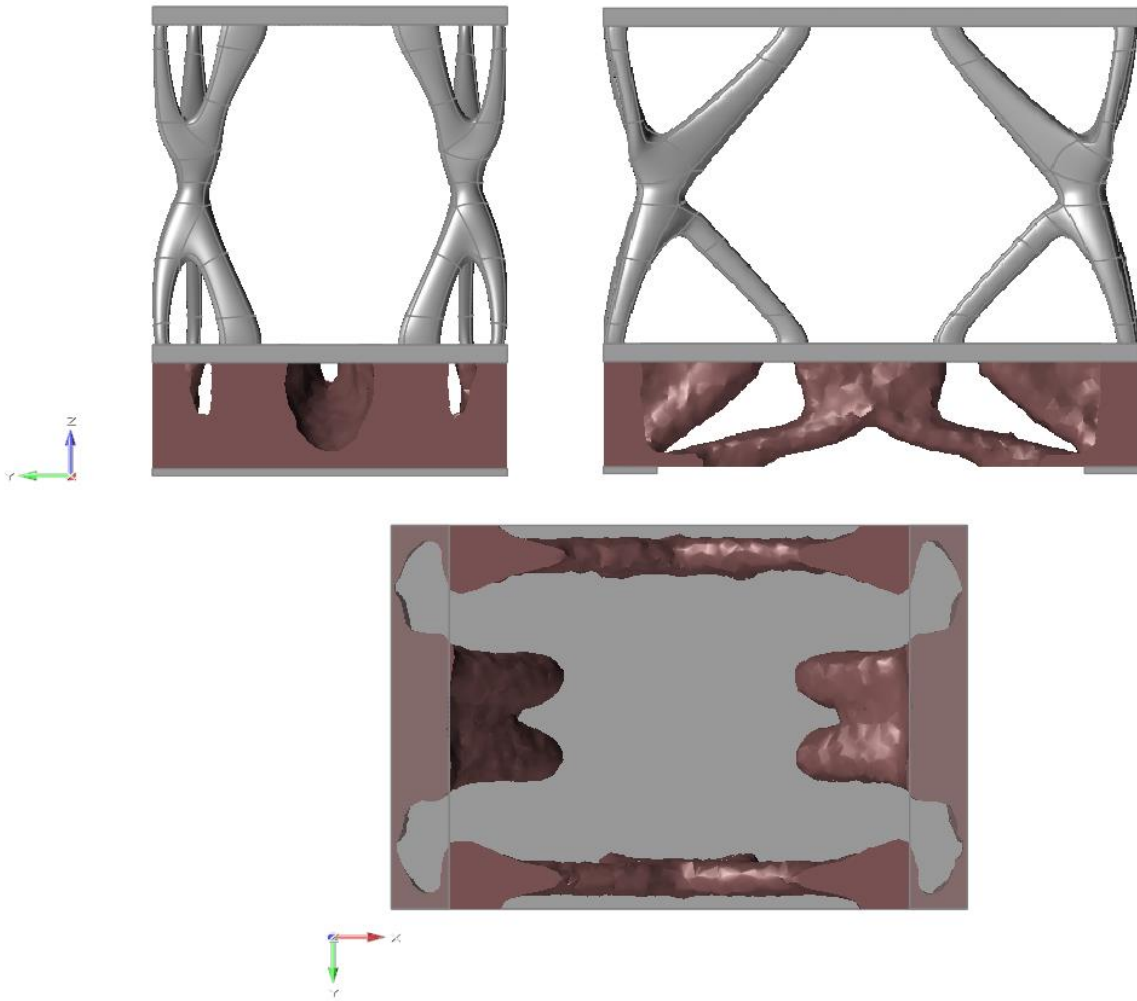


Figure 58 - Support base opt - maxstiff20% - Orthogonal views

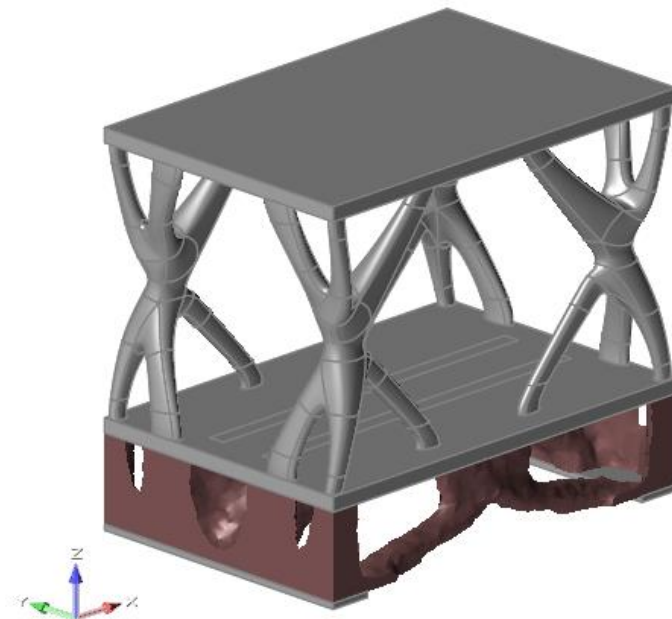


Figure 59 - Support base opt - maxstiff20% - Isometric view

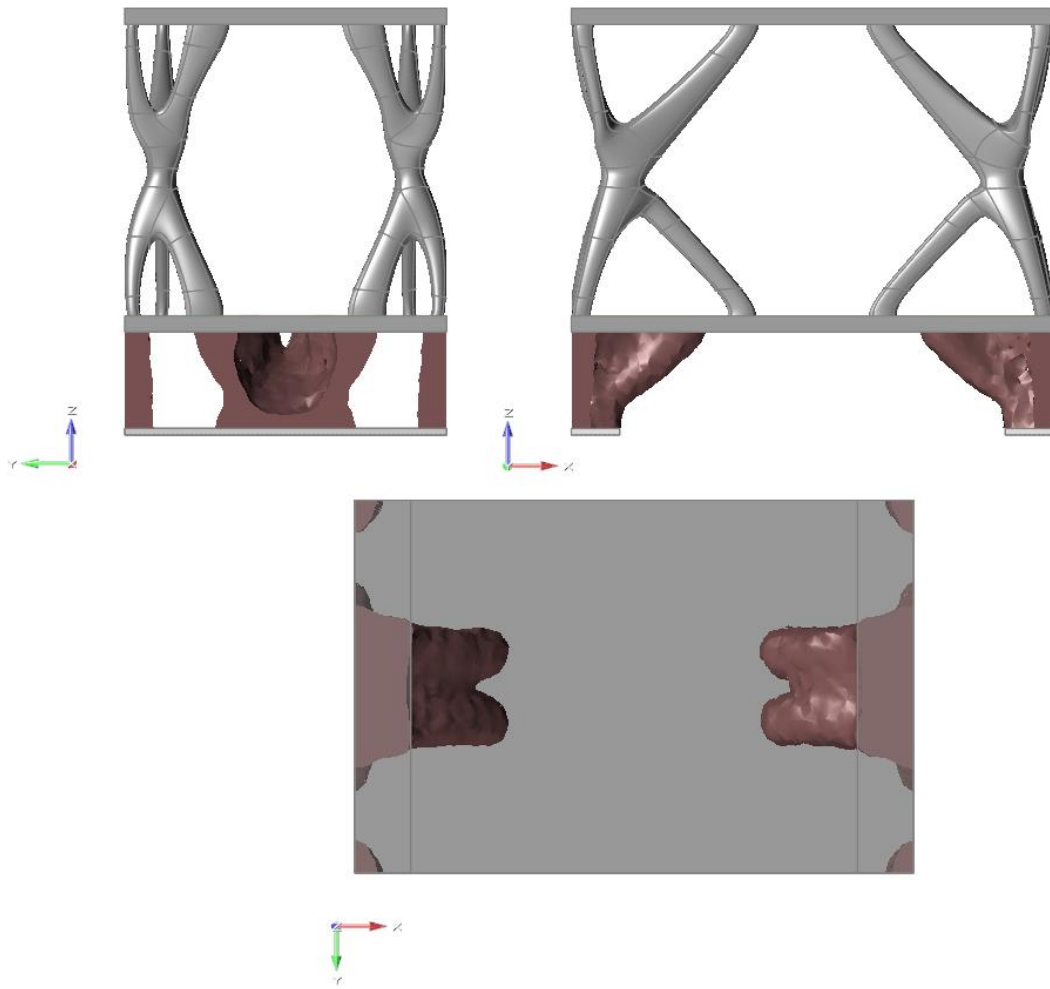


Figure 60 - Support base opt - maxstiff10% - Orthogonal views

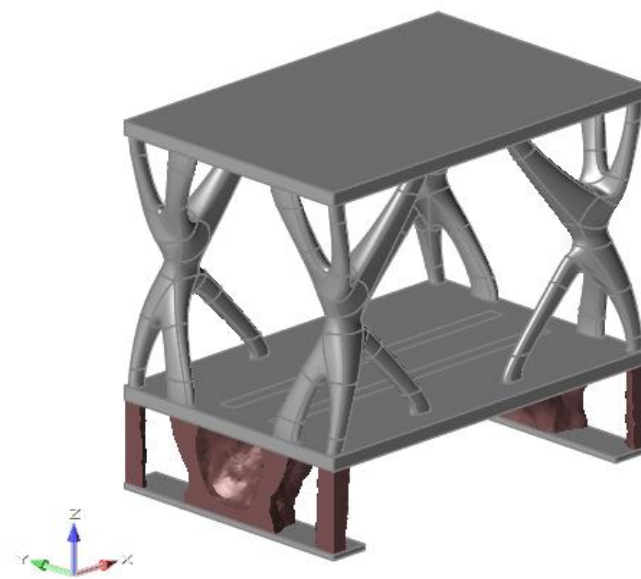


Figure 61-Support base opt - maxstiff10% - Isometric view

From Figure 58 to 61 it is possible to appreciate the results of the optimization obtained from the support base for a percentage of the design space's volume respectively equal to 20% (Figure 58 and 59) and 10% (Figure 60 and 61). It seems clear that the main cell has to be sustained both in the external (especially in Figure 58) and in the internal zone, just in correspondence of the guideways placed on the bottom plate. As well as the main cell, the supporting elements are tilted upwardly from the zone of support reaching the bottom plate of the non-design space.

For each of the two models, a static analysis was performed, and the values of the most relevant parameters were collected in Table 8.

Mechanical properties of the optimized structure's concept						
Name	Mass [kg]	DeltaMass%	Max VM stress [MPa]	Max resultant displacement [μm]	Minimum safety factor	Density Cut-off value
maxstiff20%	831	-27.6	0.62	8.03	76.5	0.6
maxstiff10%	694	-41.9	0.63	9.1	77.3	0.6

Table 8 - Mechanical properties of the optimized structure's concept

7. Re-construction and analysis of the optimized model

This chapter is meant to explain how the concept structure obtained from the topology optimization process was converted into a manufacturable geometry. The idea was to maintain the original shape and dimension of the non-design space of model 3, trying to find a way to reproduce as closely as possible the geometry of the optimized design space.

Recalling the properties described in chapter 6.4, the non-design space is made by two granite plates, each having dimension of 1500x1000x50 mm. By taking into account the ISO 8512-2 Standards [9], which define the manufacturing rules for surface plates made by cast iron or granite, it is not possible to manufacture a granite plate of such dimensions without incurring in problems of lack of stability, poor accuracy and surface flatness, which on the contrary, are highly required features for the application of this study case.

In order to overcome this problem, a fully aluminium-made structure was designed, trying to find a compromise between the mass reduction and the maximum resultant displacement achievable.

7.1. Aluminium structure

The first proposed solution (Figure 62 and 63) faithfully replicates the geometry of the optimized main cell and support base, it makes use of the elements present in the original model but with different sizes, such as the four pillars and the two support base blocks, having dimensions depicted in Figure 64. In order to reproduce the tilted elements which were present in the main cell optimization, the choice was to use aluminium profiles connected with the other structural elements by means of adjustable joints, which allows the regulation of the tilting profile for a 180° angle and, at the same time, guarantee high tightening torque. Geometry and dimensions of these elements are collected in Figure 65.

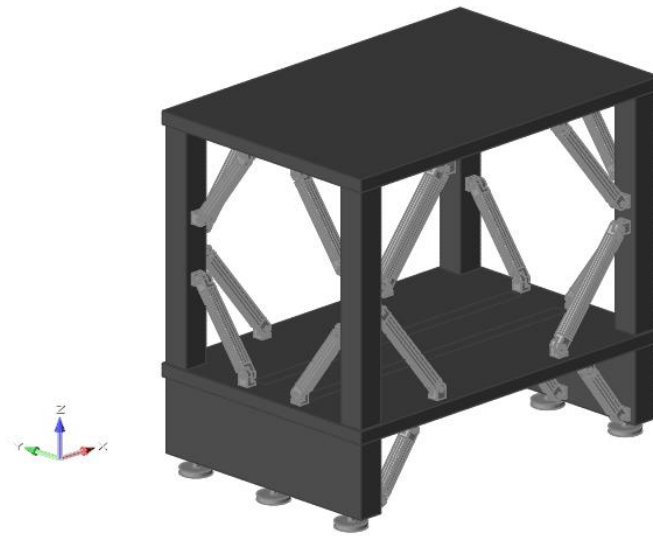


Figure 62 - Al structure - Isometric view

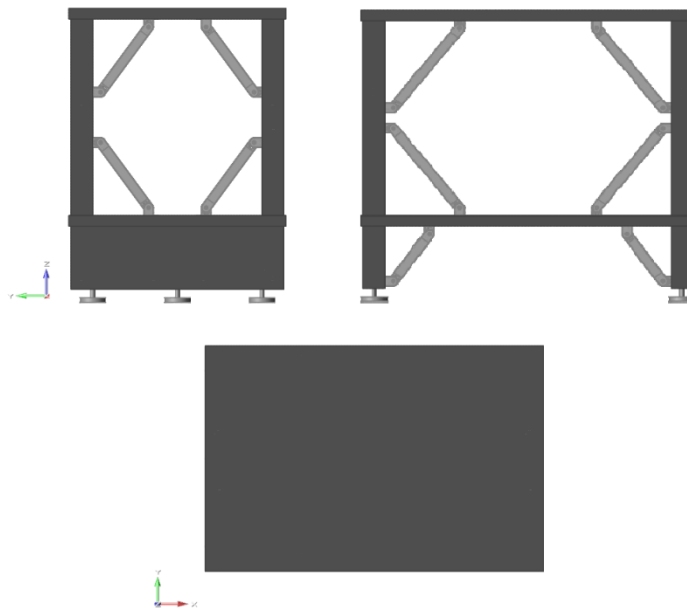


Figure 63 - Al structure - Orthogonal views

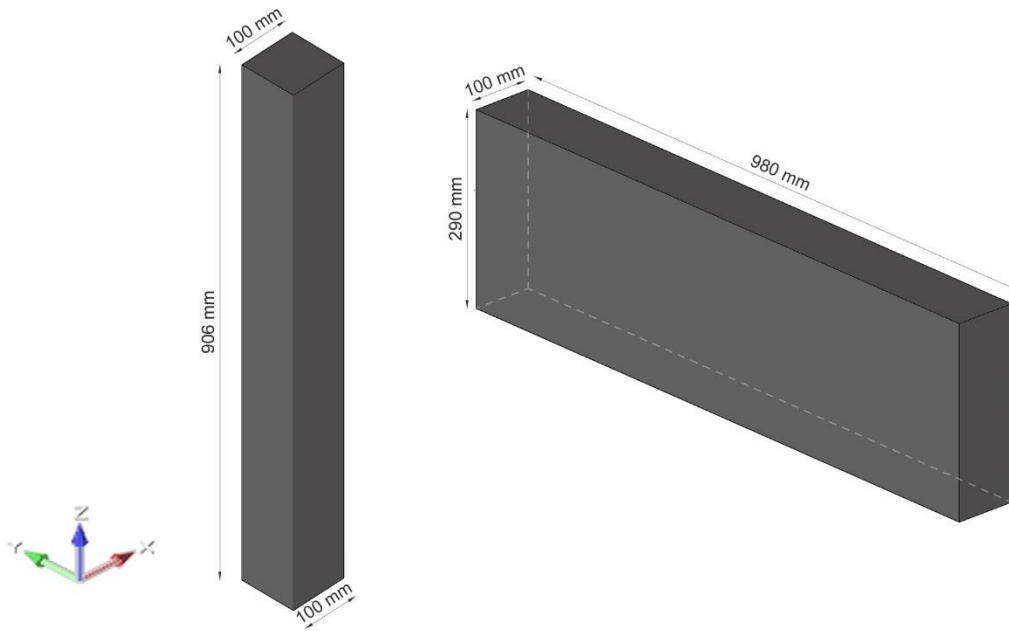


Figure 64 - Pillar and support base block's dimensions

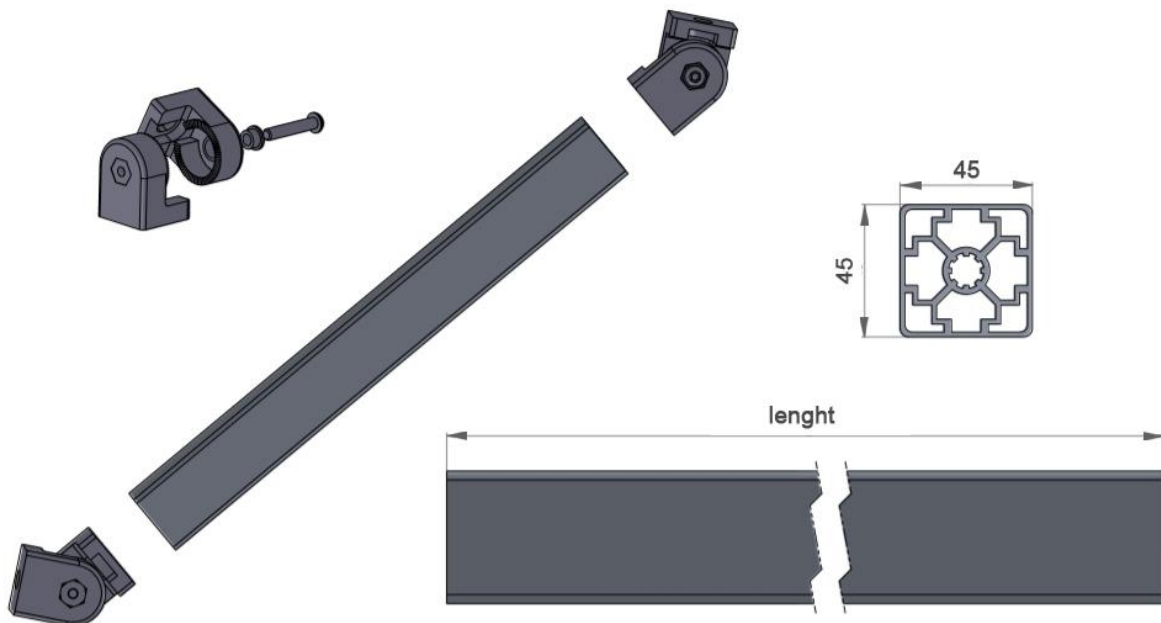


Figure 65 - Tilted elements - Geometry and dimensions

In order to replicate in the best way possible the physical properties of granite in a matter of surface finishing and stability, a particular aluminium alloy was used to produce the top and bottom plates: the 5083 Al-alloy (EN AW 5083 AlMg4,5Mn). It allows producing precision casting plates, milled and protected on both sides having low porosity content, excellent machinability and dimensional stability, good weldability and corrosion resistance. Table 9 collects the most relevant features of the 5083 Al-alloy.

5083 Aluminium - Magnesium alloys casting precision plates					
Density	Young's modulus	Yield strength	Linear expansion coefficient	Roughness	Flatness tolerance
[kg/dm^3]	[GPa]	[MPa]	[$10^{-6}/K$]	[μm]	[mm/m]
2.66	71	110	24.2	0.4	0.13

Table 9 - Physical and Mechanical properties of 5083 Al-alloy

In the next pages are presented other three different solutions, the first two are the result of the evolution of the structure already described, with the goal to maximize the performances achievable. The last one instead, is a hybrid structure, made by using granite and aluminium together. For each of the proposed solution frequency and static analysis were performed, using the same exact condition of the one performed on the original structure, in order to be able to compare the data of the new models with the original one. These data are presented respectively in Table 10 and 11, at the very end of this chapter.

7.2. Aluminium structure V2

The only difference between this structure and the first one can be observed in the geometry of the top and bottom plates, where, as it can be seen from Figure 66, part of the material has been removed from the central zone, reminding the geometry of the original model.

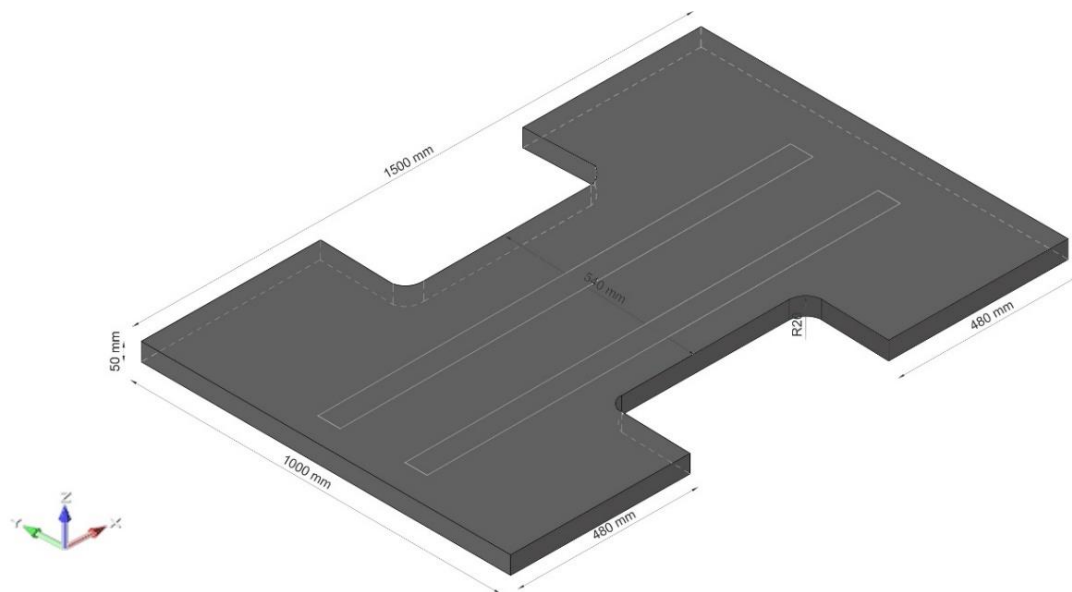


Figure 66 - Al structure V2 - Top and bottom plate's dimensions

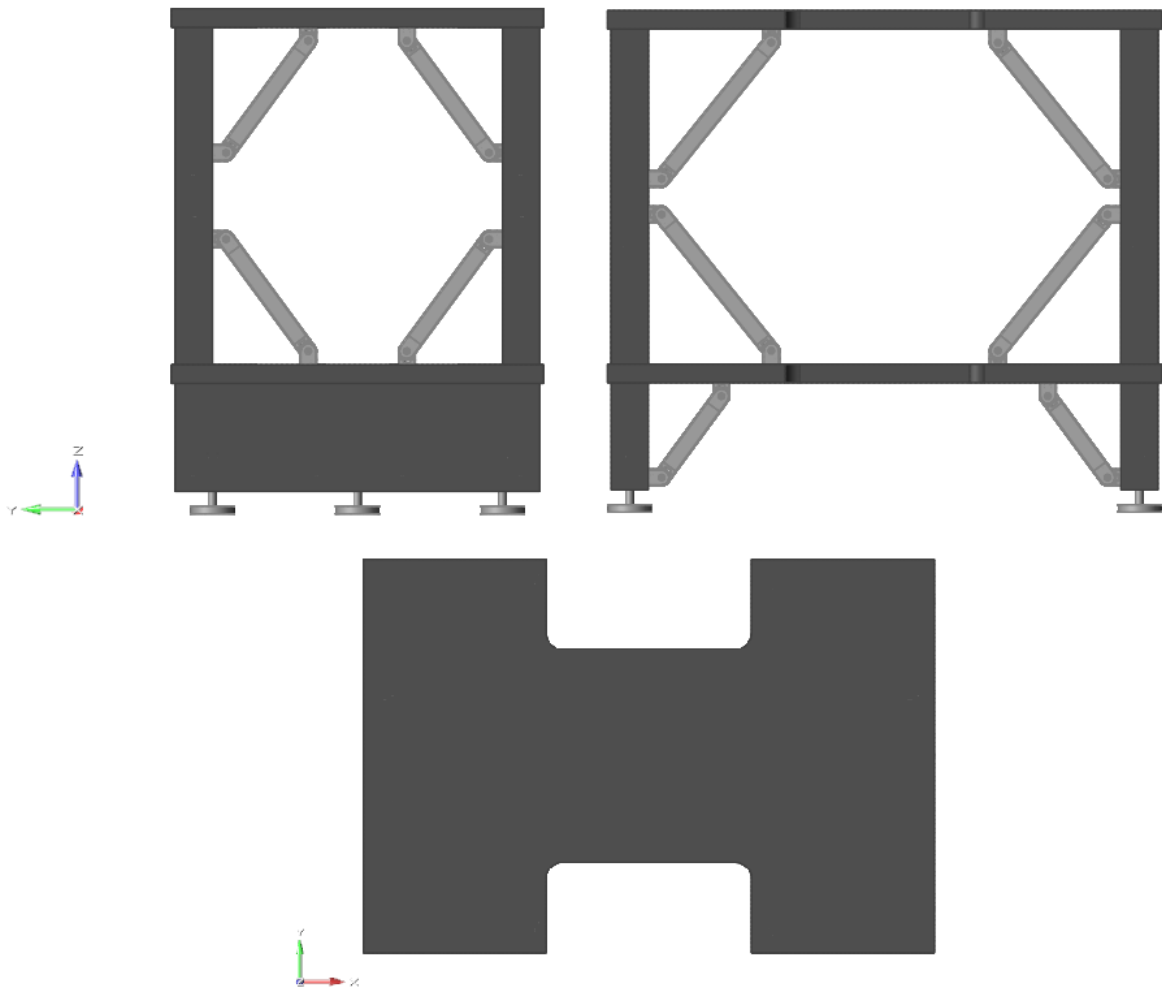


Figure 67 - AI structure V2 - Orthogonal views

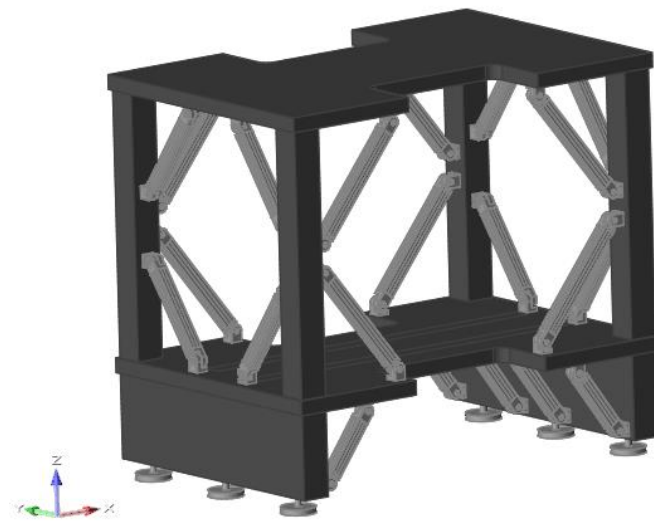


Figure 68 - AI structure V2 - Isometric view

7.3. Aluminium structure V3

This third version of the structure has been proposed with the intention to improve the mechanical properties with respect to the one observed for the first two models. From the many attempts done in order to find a better compromise between the mass reduction and the increase in displacement, it has been observed that a slight increase in the plate's thickness helps to achieve better performances. Figure 69 describes the dimensions of the components of this new version of the structure, of which the most relevant are: the change in the plate's thickness from 50 to 80 mm and the increase of the base of the pillars from 100x100 mm to 120x120 mm.

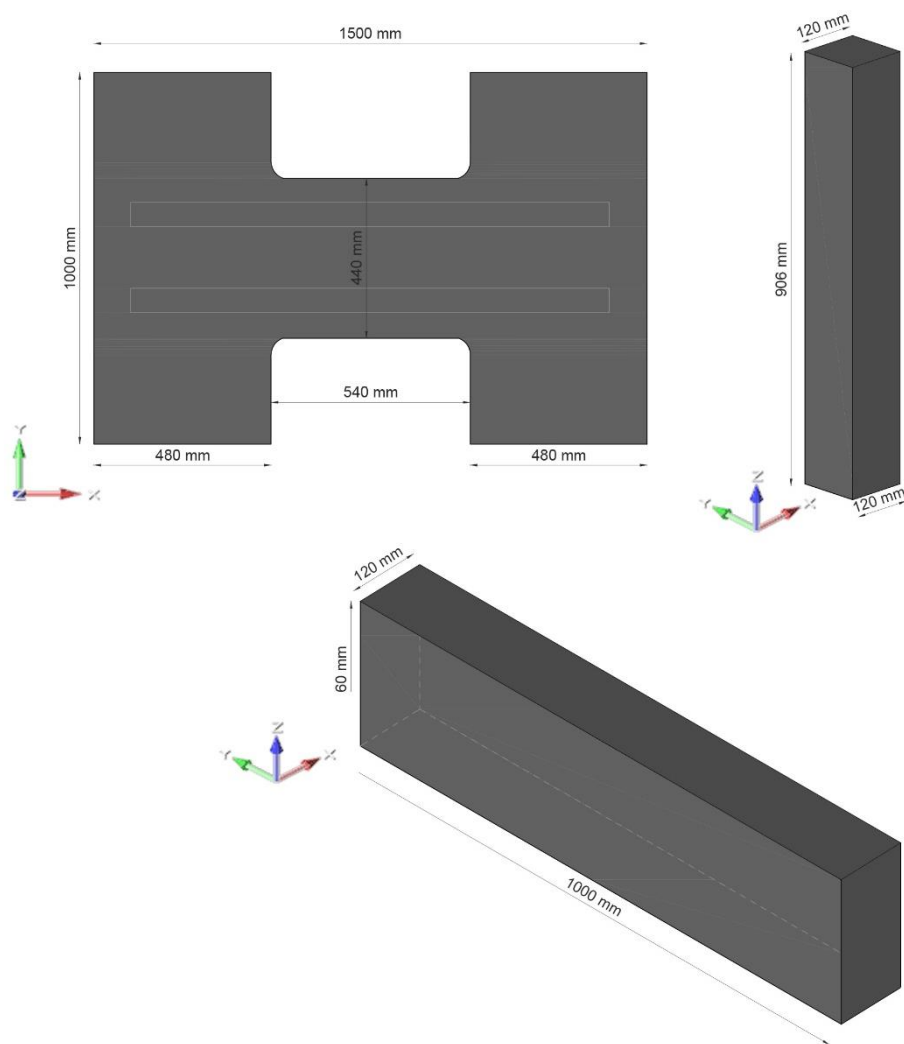


Figure 69 - Al structure V3 - Components' dimension

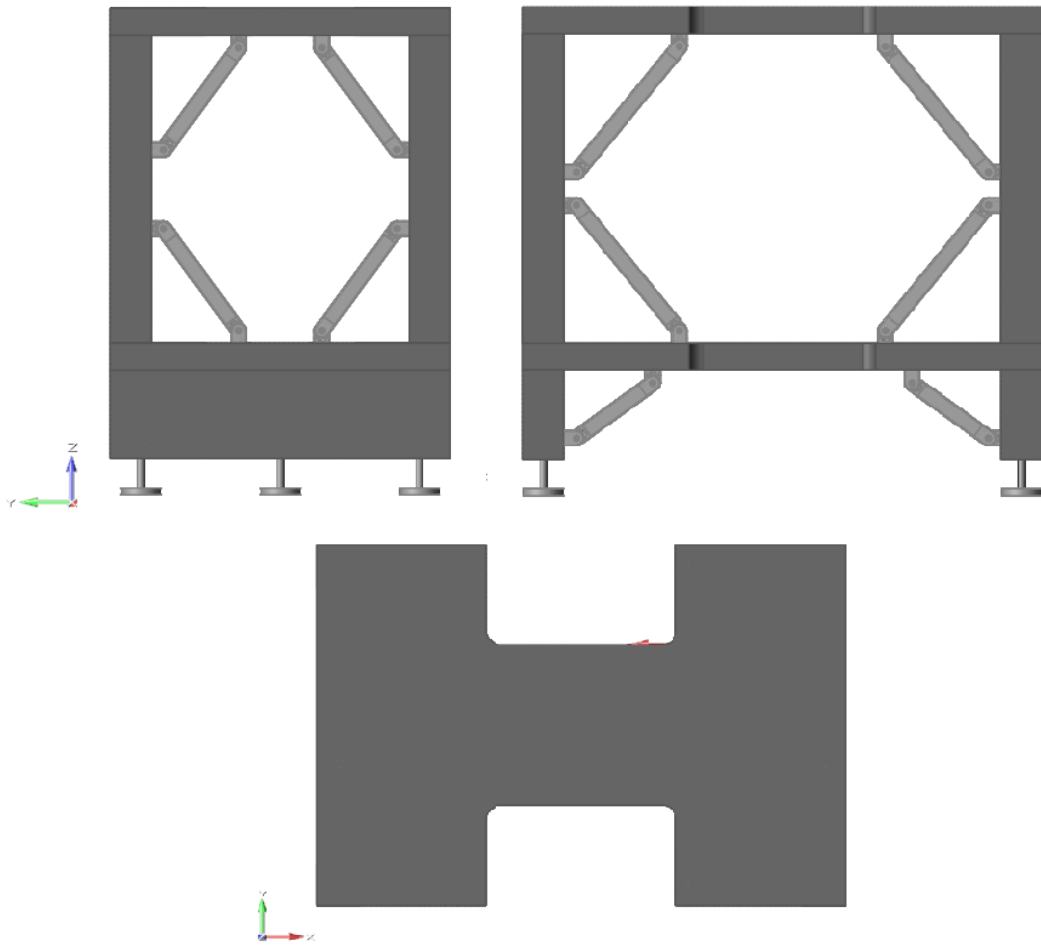


Figure 70- Al structure V3 - Orthogonal views

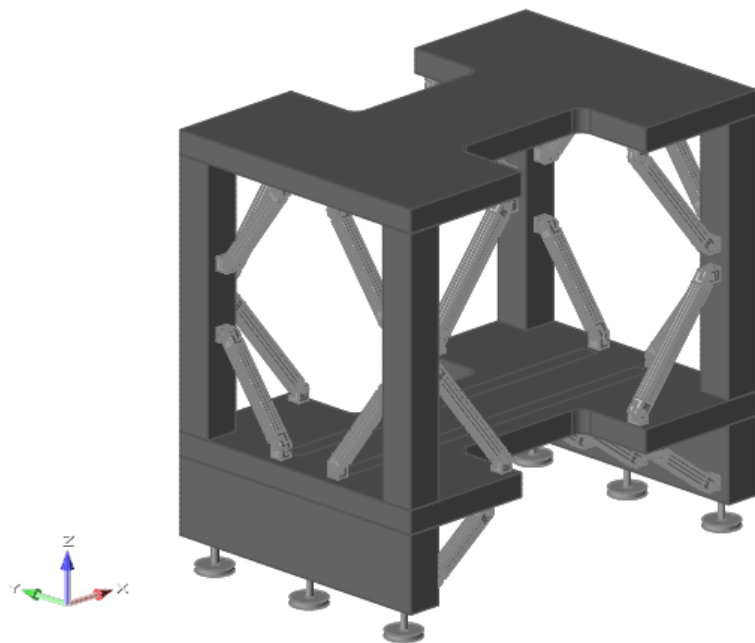


Figure 71- Al structure V3 - Isometric view

As already mentioned at the beginning of this chapter, the manufacturing constraint given by the ISO 8512-2 didn't allow to use a granite plate of such a thickness as the one used in the models before, thus leading to the use of a particular aluminium-alloys for the production of the structure's components. Even though aluminium's properties allow obtaining a lighter and still performing structure, there are some inevitable issues that have to be taken into account in the stage of choosing which is the best solution among those proposed, such as:

- Aluminium's thermal expansion coefficient is much higher than the granite's one, thus affecting the thermal and dimensional stability of the structure, in particular in specified areas where thermal gradients are present during the system's operation.
- The values of surface flatness and roughness obtained by using the 5083 Al-alloy's precision plate, even if of higher grade with respect to any other type of metallic material solution, are still comparable but lower than the one offered by the granite, which can affect negatively the repeatability and accuracy of the tests performed.

For this reason, it seemed worth trying to find a solution able to overcome the issues just described and, at the same time, capable to meet the requirement of lighter but still performing structure.

7.4. Hybrid structure

The aim of this solution is, as already mentioned, to maintain the excellent characteristics of granite and, at the same time, to use the hints obtained from the optimization process to achieve a reduction of mass for the structure. In order to do this, it was necessary to compute which was the minimum allowable value of granite plate's thickness able to meet the requirement of stability and surface finishing imposed by the ISO 8512-2 for this application. Regarding the tilted elements of the structure, the same technology of the cases formerly presented was used, taking into high consideration the connection methods between the granite and the adjustable joints, since as asserted by the Standard, the use of metal inserts in the granite plates can cause distortion due to differential expansion [9]. Figure 72 reports the most relevant dimension of the structure's components, Figure 73 and 74 instead depict its orthogonal and isometric view.

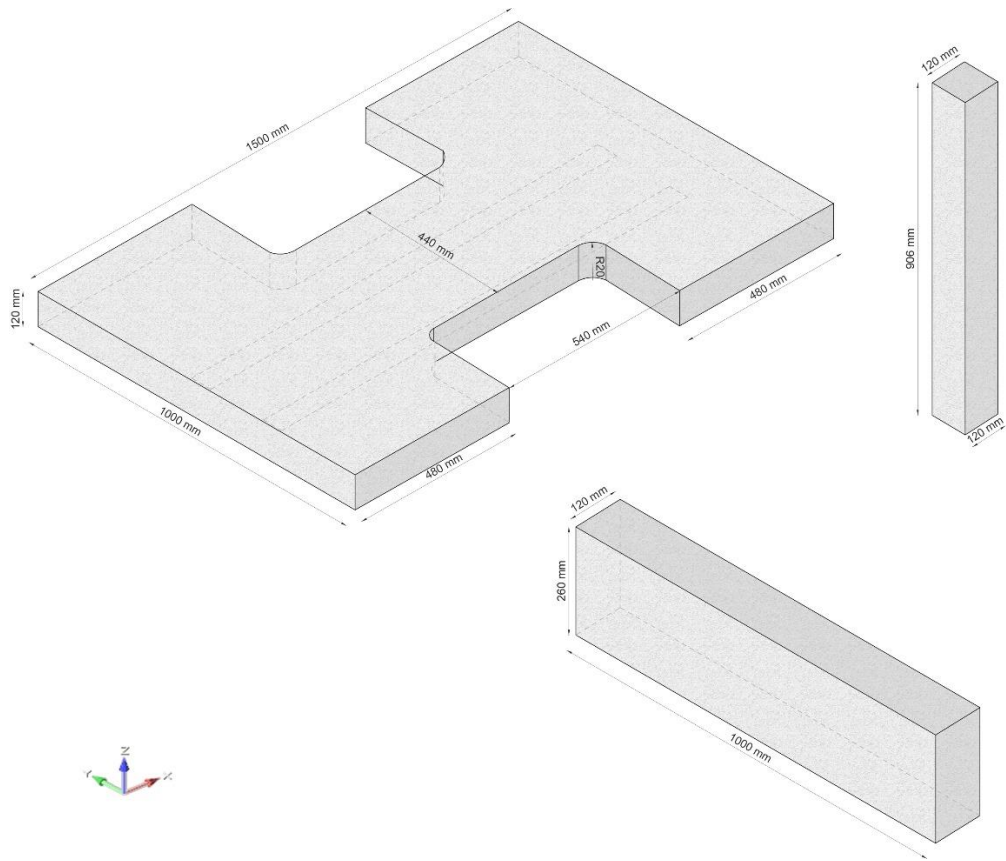


Figure 72 - Hybrid structure - Component's dimensions

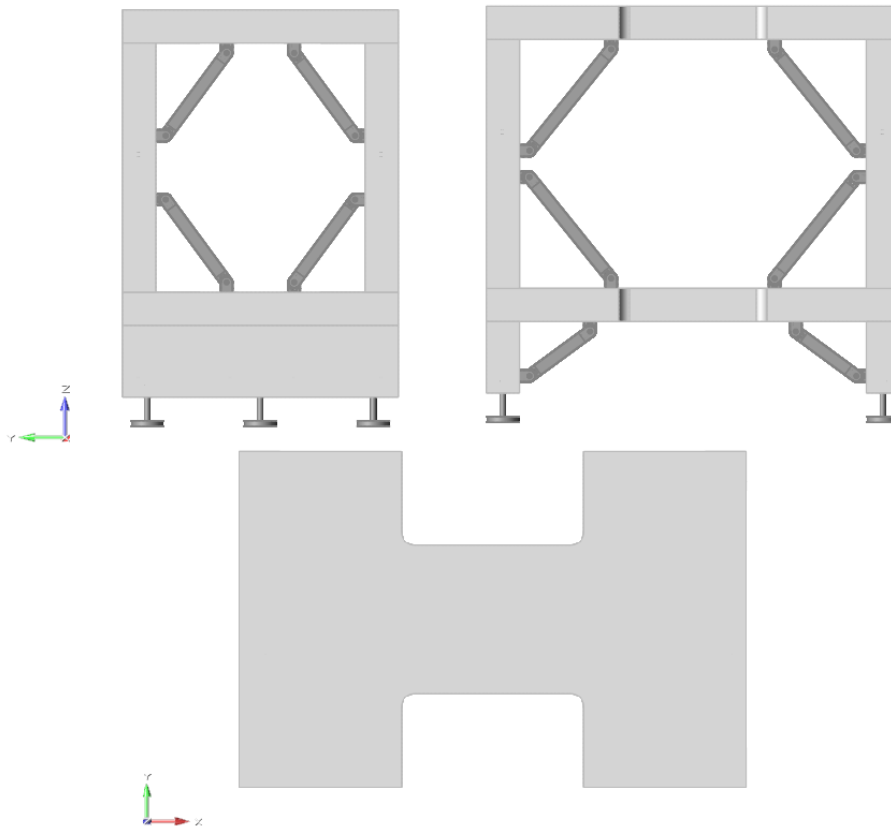


Figure 73- Hybrid structure - Orthogonal views

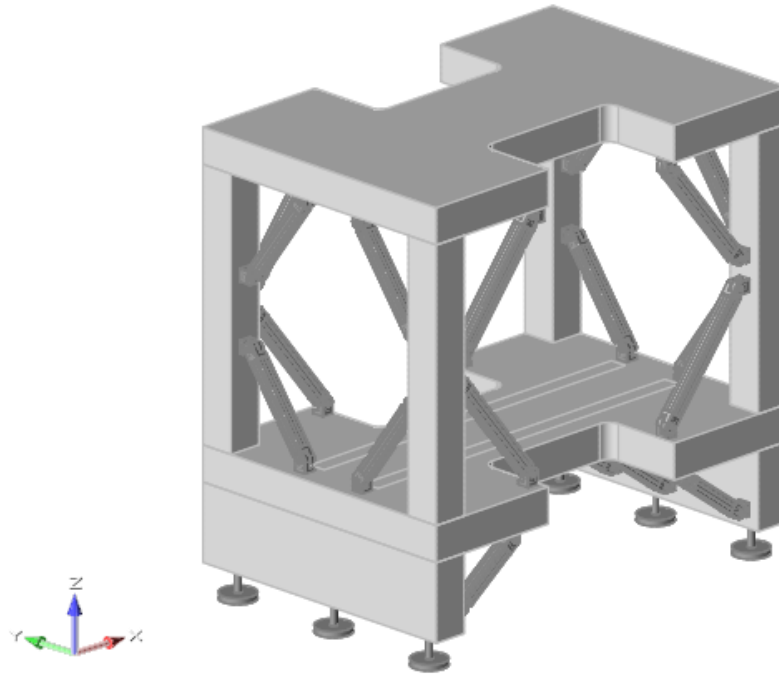


Figure 74 - Hybrid structure - Isometric view

As already mentioned, for each of the structure a set of static and modal analysis was performed, imposing the same type of loads and constraints used for the analysis of the original, in such a way to have a set of parameter to be compared. Table 10 lists the natural frequency values for the first ten modes of the structure, whereas Table 11 shows the most relevant key performance indicators.

Final solutions' natural frequencies comparison					
Mode #	AI structure [Hz]	AI structure V2 [Hz]	AI structure V3 [Hz]	Hybrid structure [Hz]	Original [Hz]
1	52,3	65,2	61,8	62,9	51,4
2	64,9	87,4	72,7	68,3	62,3
3	94,24	116,7	100	96,7	88,3
4	129,3	228,8	162,3	229,3	183,9
5	201,3	274,9	293,8	312,9	251,1
6	211,6	298,5	298,6	347,4	298,8
7	223,3	301,3	318	388,1	303
8	269,6	336,3	365,8	397,9	316,7
9	275,5	344,9	374,3	407,2	370,7
10	299,7	407,6	374,8	436,9	393,3

Table 10 - Natural frequencies comparison

From the analysis of the data in the table above it is possible to notice a common increasing trend of the value of natural frequencies, especially for “Al structure V3” and “Hybrid structure”, thus meaning that the overall ratio between the stiffness and the mass has increased with respect to the original one. Such a behaviour can be legitimated by the use of Aluminium alloys, having higher elastic modulus with respect to the granite and by the simultaneous decrease of the total mass of the structure.

Final solutions’ performances comparison					
Model	Mass <i>[kg]</i>	Mass reduction	Maximum resultant displacement <i>[μm]</i>	Maximum Von Mises stress <i>[MPa]</i>	Minimum factor of safety
Al structure	668.4	53 %	38.24	108.4	6.8
Al structure V2	604	57.6 %	48.69	139.4	20.7
Al structure V3	837.4	41.2 %	28.9	102	20.9
Hybrid	1086.8	23.6 %	20.44	72.56	12.7
Original	1423.6	/	13.95	98.8	7.6

Table 11 - Final solutions' performances comparison

From the comparison of the mechanical performances of the solution proposed with the one of the original structure it is possible to state that, by striking a balance between the mass reduction and the increase in the maximum resultant displacement, “Al structure V3” and “hybrid structure” are the one to be seriously taken into consideration for the further development of this study, since they allow to obtain a significant reduction in mass without excessively decreasing the mechanical performances of the system.

8. Conclusions

This piece of work shows how it is possible to use the topology optimization's tool in order to find a solution to the mass reduction problem, managing to reduce or even to completely remove the re-design stage from the product's cycle. On the contrary, such a method produces, as a result, geometries not always easily manufacturable with the conventional production methods, especially in this case where the study case is a granite articulated structure with very strict functional requirements, for which relatively new technologies such as 3D-printing or additive manufacturing are not suitable. Thus particular attention was made to the material to be used, to the joining techniques and to the issues relative to surface flatness, thermal and dimensional stability, which are essential parameters to take into consideration.

As a final result, four different solutions were proposed, two of which present the most promising performances, considering a compromise between the mass reduction obtained and the increase in the value of maximum resultant displacement, chosen at the start of this process as a reference value for the comparison with the original model.

Both models, "Al structure V3" and "Hybrid structure", with their strengths and weaknesses, represent a valid solution to the problem faced during this thesis project, and only further analysis can determine which of the two can guarantee the best performances.

Considering that the preliminary analysis performed onto the original model can be described as a simplification of the actual conditions, in a future perspective, for the purpose to complete the work done so far, it will be helpful to implement a set of experimental tests with some accelerometer connected to the structure with a consequent dynamic analysis in order to understand the exact behavior of the system under the effect of the acting loads. Furthermore, taking into consideration the different behaviour of the aluminium with respect to the granite, under the effect of a thermal gradient, a set of thermal analysis will help to understand the actual performances of the system, for both the final solutions proposed.

Bibliography

- [1] "Cambridge Dictionary," [Online]. Available: <https://dictionary.cambridge.org/>.
- [2] "Spea.com," [Online]. Available: <https://www.spea.com/who-we-are/>.
- [3] K. Kovler, "Science Direct," 2012. [Online]. Available: <https://www.sciencedirect.com/topics/materials-science/granite>.
- [4] J. G. Gordon, Structures or Why Things Don't Fall Down, Baltimore: Penguin, 1978.
- [5] "Wikipedia," [Online]. Available: https://en.wikipedia.org/wiki/Computer-aided_technologies.
- [6] Altair Engineering Inc., Practical Aspects of Structural Optimization., 2015.
- [7] M. P. Bendsoe and S. Ole, Topology Optimization: Theory, Methods and Applications, Berlin: Springer., 2009.
- [8] G. Mudigonda, 27 October 2016. [Online]. Available: <https://blog.altair.com/thought-leader-thursday-five-common-mistakes-made-running-topology-optimization/>.
- [9] International Organization for Standardization, November 1990. [Online]. Available: <https://www.iso.org/home.html>.